Tracing the cosmic velocity field at $z \sim 0.1$ from galaxy luminosities in the SDSS DR7

Martin Feix,[1,*] Adi Nusser,[1,2,†] and Enzo Branchini[3,4,5,‡]

[1] *Department of Physics, Israel Institute of Technology - Technion, Haifa 32000, Israel*
[2] *Asher Space Science Institute, Israel Institute of Technology - Technion, Haifa 32000, Israel*
[3] *Department of Physics, Università Roma Tre, Via della Vasca Navale 84, Rome 00146, Italy*
[4] *INFN Sezione di Roma 3, Via della Vasca Navale 84, Rome 00146, Italy*
[5] *INAF, Osservatorio Astronomico di Roma, Monte Porzio Catone, Italy*

arXiv:1405.6710v2 [astro-ph.CO] 25 Aug 2014

Spatial modulations in the distribution of observed luminosities (computed using redshifts) of $\sim 5\times10^5$ galaxies from the SDSS Data Release 7, probe the cosmic peculiar velocity field out to $z \sim 0.1$. Allowing for luminosity evolution, the r-band luminosity function, determined via a spline-based estimator, is well represented by a Schechter form with $M^\star(z)-5\log_{10}h = -20.52-1.6(z-0.1)\pm0.05$ and $\alpha^\star = -1.1\pm0.03$. Bulk flows and higher velocity moments in two redshift bins, $0.02 < z < 0.07$ and $0.07 < z < 0.22$, agree with the predictions of the ΛCDM model, as obtained from mock galaxy catalogs designed to match the observations. Assuming a ΛCDM model, we estimate $\sigma_8 \approx 1.1\pm0.4$ for the amplitude of the linear matter power spectrum, where the low accuracy is due to the limited number of galaxies. While the low-z bin is robust against coherent photometric uncertainties, the bias of results from the second bin is consistent with the $\sim 1\%$ magnitude tilt reported by the SDSS collaboration. The systematics are expected to have a significantly lower impact in future datasets with larger sky coverage and better photometric calibration.

Keywords: Cosmology: theory, observations, large-scale structure of the universe, dark matter, redshift surveys

I. INTRODUCTION

In recent years, the amount of available extragalactic data has helped to establish a comprehensive picture of our Universe and its evolution [e.g. 1–4]. These data, by and large, have enforced the standard cosmological paradigm where initial perturbations in the mass density field grow via gravitational instability and eventually form the cosmic structure we observe today. The clustering process is inevitably associated with peculiar motions of matter, namely deviations from a pure Hubble flow. On large scales, these motions exhibit a coherent pattern, with matter generally flowing from underdense to overdense regions. If galaxies indeed move much like test particles, they should appropriately reflect the underlying peculiar velocity field which contains valuable information and, in principle, could be used to constrain and discriminate between different cosmological models.

Usually relying on galaxy peculiar velocities estimated from measured redshifts and distance indicators, most approaches in the literature have focused on extracting this information within local volumes of up to $100h^{-1}$ Mpc and larger centered on the Milky Way [e.g., 5–14]. Common distance indicators are based on well-established relations between observable intrinsic properties of a given astronomical object, where one of them depends on the object's distance. A typical example is the Tully-Fisher relation [15] between rotational velocities of spiral galaxies and their absolute magnitudes. Due to observational challenges, the number of galaxies in distance catalogs is relatively small compared to that of redshift catalogs, limiting the possibility of exploring the cosmological peculiar velocity field to low redshifts $z \sim 0.02$–0.03. Moreover, all known distance indicators are potentially plagued by systematic errors [16, 17] which could give rise to unwanted biases in the inferred velocities and thus renders their use for cosmological purposes less desirable.

To probe the flow of galaxies at deeper redshifts, one needs to resort to non-traditional distance indicators. One method, for instance, exploits the kinetic Sunyaev-Zel'dovich effect to measure the cosmic bulk flow, i.e. the volume average of the peculiar velocity field, out to depths of around 100–$500h^{-1}$ Mpc [e.g, 18–21]. Another strategy is based on the apparent anisotropic clustering of galaxies in redshift space which is commonly described as redshift-space distortions. This effect is a direct consequence of the additional displacement from distances to redshifts due to the peculiar motions of galaxies, and it yields reliable constraints on the amplitude of large-scale coherent motions and the growth rate of density perturbations [e.g., 22–25].

Galaxy peculiar motions also affect luminosity estimates based on measured redshifts, providing another way of tackling the problem. Since the luminosity of a galaxy is independent of its velocity, systematic biases in the estimated luminosities of galaxies can be used to explore the peculiar velocity field. The idea has a long history. It was first adopted to constrain the velocity of the Virgo cluster relative to the Local Group by correlating the magnitudes of nearby galaxies with their redshifts [26]. Although in need of very large galaxy numbers to be effective, methods based on this idea use only measured galaxy luminosities and their redshifts to

* Electronic address: mfeix@physics.technion.ac.il
† Electronic address: adi@physics.technion.ac.il
‡ Electronic address: branchin@fis.uniroma3.it

derive bounds on the large-scale peculiar velocity field. Therefore, these methods do not require the use of traditional distance indicators and they are also independent of galaxy bias. Using the nearly full-sky 2MASS Redshift Survey (2MRS) [27], for example, this approach has recently been adopted to constrain bulk flows in the local Universe within $z \sim 0.01$ [28, 29]. Furthermore, it has been used to determine the current growth rate of density fluctuations by reconstructing the full linear velocity field from the clustering of galaxies [30, 31].

Here we seek to apply this luminosity-based approach to obtain peculiar velocity information from galaxy redshifts and apparent magnitudes of the Sloan Digital Sky Survey (SDSS) [32]. The goals of our analysis are:

- A demonstration of the method's applicability to datasets with large galaxy numbers.
- An updated estimate of the r-band luminosity function of SDSS galaxies at $z \sim 0.1$, accounting for evolution in galaxy luminosities.
- Novel bounds on bulk flows and higher-order moments of the peculiar velocity field at redshifts $z \sim 0.1$.
- First constraints on the angular peculiar velocity power spectrum and cosmological parameters without additional input such as galaxy clustering information.

The paper is organized as follows: we begin with introducing the luminosity method and its basic equations in section II. In section III, we then describe the SDSS galaxy sample used in our analysis, together with a suite of mock catalogs which will allow us to assess uncertainties and known systematics inherent to the data. After a first test of the method, we attempt to constrain peculiar motions in section IV, assuming a redshift-binned model of the velocity field. Because of the mixing between different velocity moments arising from the SDSS footprint, bulk flow measurements are interpreted with the help of galaxy mocks. Including higher-order velocity moments, we proceed with discussing constraints on the angular velocity power in different redshift bins and their implications. As an example of cosmological parameter estimation, we further infer the quantity σ_8, i.e. the amplitude of the linear matter power spectrum on a scale of $8h^{-1}$ Mpc, and compare the result to the findings from the corresponding mock analysis. Other potential issues and caveats related to our investigation are addressed at the section's end. In section V, we finally summarize our conclusions and the method's prospects in the context of next-generation surveys. For clarity, some of the technical material is separately given in an appendix. Throughout the paper, we adopt the standard notation, and all redshifts are expressed in the rest frame of the cosmic microwave background (CMB) using the dipole from ref. [33].

II. METHODOLOGY

A. Variation of observed galaxy luminosities

In an inhomogeneous universe, the observed redshift z of an object (a galaxy) is generally different from its cosmological redshift z_c defined for the unperturbed background. To linear order in perturbation theory, one finds the well-known expression [34]

$$\begin{aligned}\frac{z-z_c}{1+z} &= \frac{V(t,r)}{c} - \frac{\Phi(t,r)}{c^2} \\ &\quad - \frac{2}{c^2}\int_{t(r)}^{t_0} \mathrm{d}t \frac{\partial\Phi\left[\hat{\boldsymbol{r}}r(t),t\right]}{\partial t} \approx \frac{V(t,r)}{c},\end{aligned} \tag{1}$$

where V is the physical radial peculiar velocity of of the object, Φ denotes the gravitational potential and $\hat{\boldsymbol{r}}$ is a unit vector along the line of sight to the object. The last step explicitly assumes low redshifts where the velocity V makes the dominant contribution.[1] Note that all fields are considered relative to their present-day values at a comoving radius of $r(t=t_0)$ and that we have substituted z for z_c in the denominator on the left-hand side of eq. (1), which simplifies part of the analysis presented below and is consistent at the linear level.

The observed absolute magnitude M, computed using the galaxy redshift z, rather than the (unknown) cosmological redshift z_c, differs from the true value $M^{(t)}$ because of the shift $\mathrm{DM}(z) - \mathrm{DM}(z_c)$ in the distance modulus $\mathrm{DM} = 25 + 5\log_{10}[D_L/\mathrm{Mpc}]$, where D_L is the luminosity distance. Hence,

$$\begin{aligned}M &= m - \mathrm{DM}(z) - K(z) + Q(z) \\ &= M^{(t)} + 5\log_{10}\frac{D_L(z_c)}{D_L(z)},\end{aligned} \tag{2}$$

where m is the apparent magnitude, $K(z)$ is the K-correction [e.g., 35], and the function $Q(z)$ accounts for luminosity evolution. Since the variation $M - M^{(t)}$ of magnitudes distributed over the sky is systematic, it can be used to gain information on the peculiar velocity field. In the following, we will discuss how this may be achieved with the help of maximum-likelihood techniques.

B. Statistical description

1. *Inference of bulk flows and other velocity moments*

Before introducing our methodology, we need to specify a suitable model of the velocity field. Although a popular option is to characterize peculiar velocities in terms

[1] The first two terms on the right-hand side of eq. (1) describe the Doppler effect and the gravitational redshift, respectively. The last one reflects the energy change of a photon passing through a time-dependent potential well and is equivalent to the late-time integrated Sachs-Wolfe effect.

of bulk flows, one could aim at a more complete description of the peculiar velocity field. Given the current data, however, a full three-dimensional estimate of the velocity field would be entirely dominated by the noise. A more promising approach is the following: first, we subdivide the galaxy data into suitable redshift bins and consider the bin-averaged velocity $\tilde{V}$. Supposing for the moment that we are dealing with a single bin, we then proceed to decompose $\tilde{V}(\hat{\boldsymbol{r}})$ (evaluated at the galaxy position $\hat{\boldsymbol{r}}$) into spherical harmonics, i.e.

$$\begin{aligned} a_{lm} &= \int \mathrm{d}\Omega \tilde{V}(\hat{\boldsymbol{r}}) Y_{lm}(\hat{\boldsymbol{r}}), \\ \tilde{V}(\hat{\boldsymbol{r}}) &= \sum_{l,m} a_{lm} Y^*_{lm}(\hat{\boldsymbol{r}}), \quad l > 0, \end{aligned} \tag{3}$$

where the sum over l is cut at some maximum value $l_{\max}$. A bulk flow of the entire volume, denoted as $\boldsymbol{v}_B$, corresponds to the dipole term ($l = 1$) in eq. (3). Building on the pioneering work of [26], for example, the analysis presented in [28] has initially been restricted to a model with $l_{\max} = 1$ when considering galaxies from the 2MRS [27].

Assuming that redshift errors can be neglected [28], we write the probability of observing a galaxy with magnitude M, given only its redshift and angular position $\hat{\boldsymbol{r}}$ on the sky, as

$$P\left(M|z, a_{lm}\right) = P\left(M|z, \tilde{V}(\hat{\boldsymbol{r}})\right) = \frac{\phi(M)}{\eta\left(M^+, M^-\right)}, \tag{4}$$

where $\phi(M)$ is the galaxy luminosity function (LF) and $\eta\left(M^+, M^-\right)$ is defined as

$$\eta\left(M^+, M^-\right) = \int_{M^+}^{M^-} \phi(M)\mathrm{d}M. \tag{5}$$

The corresponding limiting magnitudes $M^\pm$ are given by

$$\begin{aligned} M^+ &= \max\left[M_{\min}, m^+ - \mathrm{DM}(z_c) - K(z) + Q(z)\right], \\ M^- &= \min\left[M_{\max}, m^- - \mathrm{DM}(z_c) - K(z) + Q(z)\right], \end{aligned} \tag{6}$$

where $m^\pm$ are the sample's limiting apparent magnitudes and the cosmological redshift z_c depends on the velocity $\tilde{V}$ and the observed redshift z because of eq. (1). The velocity model enters the expression for the limiting magnitudes $M^\pm$ since it induces a shift in the distance modulus. The coefficients a_{lm} of the flow modes can, therefore, be inferred by maximizing the total log-likelihood obtained from the sum over all galaxies in a sample, i.e. $\log P_{\mathrm{tot}} = \sum \log P_i$. The rational for this is to find the set of a_{lm} which minimizes the spread in the observed magnitudes [28]. The spherical harmonics provide an orthogonal basis only in the case of an all-sky survey, and the partial sky coverage of the SDSS implies that the inferred moments will not be statistically independent. For example, a quadrupole velocity mode ($l = 2$) would contaminate the estimate of a bulk flow $\boldsymbol{v}_B$, which must be taken into account when interpreting any results. The monopole term ($l = 0$) is completely degenerate with an overall shift of the magnitudes, and hence it is not included.

If the number of available galaxies is large enough, the central limit theorem implies that P_{tot} becomes approximately normal, and we have

$$\log P_{\mathrm{tot}}\left(\boldsymbol{d}|\boldsymbol{x}\right) = -\frac{1}{2}\left(\boldsymbol{x} - \overline{\boldsymbol{x}}\right)^{\mathrm{T}} \boldsymbol{\Sigma}^{-1}\left(\boldsymbol{x} - \overline{\boldsymbol{x}}\right), \tag{7}$$

where $\boldsymbol{x}$ is a vector of all model parameters, $\overline{\boldsymbol{x}}$ is the corresponding mean, $\boldsymbol{d}$ denotes the data (or Bayesian evidence), and $\boldsymbol{\Sigma}$ is the covariance matrix describing the expected error of our estimate. We have numerically verified that this approximation is extremely accurate for the SDSS which comprises several hundred thousands of galaxies. The distribution's mean in eq. (7) simply corresponds to the maximum-likelihood estimate $\hat{\boldsymbol{x}}^{\mathrm{ML}}$ of the vector $\boldsymbol{x}$, and $\boldsymbol{\Sigma}$ can be estimated either by inverting the observed Fisher matrix $\mathbf{F}$ which is defined as $\mathbf{F}_{\alpha\beta} = -\partial \log P_{\mathrm{tot}}/(\partial x_\alpha \partial x_\beta)$ evaluated at the maximum value $\hat{\boldsymbol{x}}^{\mathrm{ML}}$ or from a realistic set of mock galaxy catalogs. The increasing number of parameters associated with the higher-order moments of $\tilde{V}$ typically renders a full numerical evaluation of $\log P_{\mathrm{tot}}$ unfeasible. A solution to this problem is based on approximating the total log-likelihood function to second order (see section IV A and appendix A for details). In the realistic application to SDSS data, the model parameters $\boldsymbol{x}$ include the coefficients a_{lm} (for each redshift bin) as well as the LF parameters. They will be determined simultaneously by maximizing $\log P_{\mathrm{tot}}$.

2. *Inference of angular velocity power spectra*

Let us now focus on large scales where linear theory is applicable. Assuming Gaussian initial conditions, the cosmological peculiar velocity field on these scales is then fully characterized by its power spectrum. The relevant quantity here is the angular velocity power spectrum $C_l = \langle |a_{lm}^2| \rangle$. Under these preliminaries, the problem of inferring the C_l becomes equivalent to the more familiar estimation of the CMB anisotropy power spectrum, and may thus be tackled with the same general techniques [36, 37]. To estimate the power spectrum, one simply maximizes the probability of observing the data given the C_l, i.e.

$$P(C_l) \equiv P\left(\boldsymbol{d}|C_l\right) \propto \int \mathrm{d}a_{lm} P\left(\boldsymbol{d}|a_{lm}\right) P\left(a_{lm}|C_l\right), \tag{8}$$

which is obtained by constructing the posterior likelihood according to Bayes' theorem and marginalizing over the a_{lm}. Here the individual a_{lm} are uncorrelated and taken to be normally distributed, i.e. one has

$$P\left(a_{lm}|C_l\right) = \prod_{l,m} \left(2\pi C_l\right)^{-1/2} \exp\left(-\frac{|a_{lm}|^2}{2C_l}\right), \tag{9}$$

and $P(\boldsymbol{d}|a_{lm})$ is derived from marginalizing $P_{\rm tot}(\boldsymbol{d}|\boldsymbol{x})$ over the remaining parameters in $\boldsymbol{x}$. Within the Gaussian approximation, carrying out the integration in eq. (8) is straightforward and the resulting expressions are presented in appendix B.

Considering a particular model like, for example, the standard ΛCDM cosmology, the C_l are fully specified by a set of cosmological parameters ζ_k. Therefore, accounting for this dependency in the prior probability, the above technique may further be used to constrain cosmological key quantities such as σ_8 from the observed peculiar velocity field alone. Given the characteristics of current galaxy redshift surveys, it is clear that these constraints will be much less tight than those obtained by other means such as CMB analysis, but still valuable as a complementary probe and consistency check.

A successful application of the method requires a large number of galaxies to beat the statistical (Poissonian) errors. The method does not require accurate redshifts and can be used with photometric redshifts to recover signals on scales larger than the spread of the redshift error. Other related maximum-likelihood approaches based on reduced input (photometric redshifts or just magnitudes) [38, 39] consider integrated quantities such as number densities, resulting in less sensitive measurements of bulk flows and higher-order moments of the peculiar velocity field.

C. Estimating the galaxy luminosity function

A reliable measurement of the galaxy LF represents a key step in our approach. A corresponding estimator should be flexible enough to capture real features in the luminosity distribution, but also physical in the sense of returning a smooth function over the range of interest. To meet these requirements, we shall adopt the spline-based estimator introduced in [29] for our analysis.[2] In this case, the unknown LF is written as a piecewise-defined function, i.e.

$$\phi(M) = \varphi_i(M), \qquad M_{i-1} \leq M < M_i, \qquad (10)$$

where φ_i is a third-order polynomial defined such that the second derivative of ϕ with respect to M is continuous on the interval $[M_0, M_{N-1}]$ and vanishes at the boundaries. The cubic spline in eq. (10) may be regarded as a generalization of the stepwise estimator originally proposed in [40], and the actual spline coefficients are determined employing the standard techniques summarized in [41]. Since there occur only polynomial expressions, derivatives and integrals of $\phi(M)$ are of particularly simple form, allowing quite an efficient evaluation of the previously defined likelihood functions. LFs which are obtained according to this procedure might exhibit spurious wiggles, especially at the corresponding bright and faint ends. As is already discussed in [29], however, these wiggles can be sufficiently suppressed by adding an appropriate penalty term to the total likelihood function or by enforcing (log-)linear behavior of $\phi(M)$ beyond suitable bright and faint magnitude thresholds. Alternatively, it is also possible to simply choose magnitude cuts and the total number of spline points in such a way that the number of galaxies in each magnitude interval is large enough to avoid this problem for all practical purposes. In the present analysis, we will follow the latter approach when maximizing the total log-likelihood.

In addition to the spline-based estimator, which is most relevant when considering real observations, we shall also use a parametric estimator that assumes a widely used Schechter form of the LF [42, 43], i.e.

$$\phi(M) \propto 10^{0.4(1+\alpha^\star)(M^\star - M)} \exp\left(-10^{0.4(M^\star - M)}\right), \quad (11)$$

where $M^\star$ and $\alpha^\star$ are the usual Schechter parameters. The normalization of $\phi(M)$ cancels in the likelihood function and does not concern us here. Although it does not provide a good fit to all datasets, the Schechter form and its corresponding estimator turn out very useful for the analysis of both mock catalogs and the real galaxy sample presented in section IV.

III. DATASETS

A. NYU Value-Added Galaxy Catalog

We will use the SDSS galaxies from the latest publicly available NYU Value-Added Galaxy Catalog (NYU-VAGC) [44].[3]. This catalog is based on the SDSS Data Release 7 (DR7) [45], and contains galaxies with a median redshift of $z \approx 0.1$, observed in five different photometric bands with magnitudes corrected for Galactic extinction according to [46]. Using Petrosian magnitudes, we decide to work with the r-band, mainly because it gives the largest spectroscopically complete galaxy sample [47, 48], which is an important factor for the statistical method we have introduced in section II. To minimize incompleteness and to exclude galaxies with questionable photometry and redshifts, we choose the subsample NYU-VAGC `safe` which contains only galaxies whose apparent r-band magnitudes satisfy $14.5 < m_r < 17.6$.[4] The subsample accounts for fiber collisions following the correction scheme `nearest`, but this is expected to be of

[2] Since the underlying principle is a reduction in the spread of observed magnitudes, even unrealistic models of the luminosity distribution should yield unbiased measurements of the velocity information [31], albeit with larger statistical errors.

[3] `http://sdss.physics.nyu.edu/vagc/`

[4] The SDSS photometry is known to exhibit small offsets from the AB magnitude system [49]. For the SDSS r-band, this amounts to a shift of around 0.01 [50] which we will take into account when calculating absolute magnitudes below.

little relevance in our analysis which should be insensitive to galaxy clustering. Also, since we are interested in minimizing systematics due to uncertainties in K-corrections and luminosity evolution (see section IV), we shall adopt the ${}^{0.1}r$-bandpass when dealing with absolute magnitudes [51], and further impose cuts on redshifts (expressed in the CMB frame) and observed absolute magnitudes M_r such that only galaxies with $0.02 < z < 0.22$ and $-22.5 < M_r - 5\log_{10} h < -17.0$ are selected. The number of galaxies contained in our final working sample is approximately 5.4×10^5 and may slightly vary, depending on the assumed background cosmology which enters the calculation of M_r through the luminosity distance. For realistic flat cosmologies with a total matter density $\Omega_m \approx 0.3$, however, these variations are typically on the order of a few hundred galaxies and thus not very significant. Since we are concerned with relatively low redshifts $z \lesssim 0.2$, we assume a linear dependence of the luminosity evolution on redshift for simplicity, i.e.

$$Q(z) = Q_0(z - z_0), \tag{12}$$

where we set the pivotal redshift $z_0 = 0.1$. Furthermore, K-corrections for individual galaxies are taken from the NYU-VAGC and have been calculated with the software package `kcorrect v4_1_4` [35]. To calculate the limiting absolute magnitudes $M^{\pm}$ in the ${}^{0.1}r$-bandpass at a given redshift z, however, we resort to a mean K-correction of the form

$$\overline{K}(z) = -2.5\log_{10}(1.1) + \sum_{i=1}^{3}\gamma_i(z-0.1)^i, \tag{13}$$

where $\gamma_1 \approx 0.924$, $\gamma_2 \approx 2.095$, and $\gamma_3 \approx -0.184$ are determined by directly fitting the individual K-corrections listed in the NYU-VAGC. When calculating the total likelihood function introduced in section II B, all galaxies are weighted according to the angular (redshift) completeness. All remaining details relevant to the analysis of the NYU-VAGC galaxy redshift data will be separately discussed in section IV A.

B. Mock galaxy catalogs

To test the performance of our approach, we resort to two different suites of galaxy mock catalogs. The first set of mocks is based on the LasDamas simulations [52] while the second one is obtained from the real NYU-VAGC dataset that we analyse in this work.

1. *LasDamas mock catalogs*

These mock galaxy catalogs are obtained by populating the LasDamas simulations [52] with artificial galaxies, using a halo occupation distribution model [e.g., 53–55] to match the observed clustering of SDSS galaxies in a wide luminosity range. The goal of these catalogs is to benchmark our method and validate its implementation, using a sample with overall characteristics (number density of objects, sky coverage, etc.) similar to that of the real catalog, ignoring all sources of systematic biases.

Here we will consider a total of 60 mocks from the public `gamma` release, modeled after a volume-limited subsample of SDSS DR7 cut at $M_r < -20$, which cover the full SDSS footprint ("North and South") and a redshift range $0.02 < z < 0.106$ with a median of $z \approx 0.08$.[5] The typical galaxy number in these mocks is around $1-1.5\times10^5$, and we shall use them as a basic test of bulk flow measurements. To this end, an observed redshift is assigned to each galaxy according to

$$cz = cz_c + V + c\epsilon_z, \tag{14}$$

where z_c corresponds to the redshift entry in the mock catalog, the radial velocity $V = \hat{\boldsymbol{r}}\cdot\boldsymbol{v}_B$ is the line-of-sight component of the bulk flow $\boldsymbol{v}_B$, and ϵ_z is a random measurement error drawn from a Gaussian distribution with $c\sigma_z = 15$ km s^{-1}.[6] Similarly, observed r-band magnitudes are assigned with the help of eq. (2), but without including the K-correction term. Assuming the linear luminosity evolution in (12) with $Q_0 = 1.6$, the true galaxy magnitudes $M^{(t)}$ are randomly extracted from the Schechter distribution given by eq. (11) with the parameters $M^\star = -20.44 + 5\log_{10} h$ and $\alpha^\star = -1.05$ [56]. Although it is irrelevant for the present purposes, this procedure ignores the masses of dark matter halos, meaning that very massive halos may host very faint galaxies and vice versa. We also add a Gaussian random error to M_r with $\sigma_M = 0.03$, and further trim the resulting mock catalogs by requiring $M_r < -20.25$ to prevent problems related to Malmquist bias. Finally, our choice of the bulk flow $\boldsymbol{v}_B$ used in the benchmark runs will be described in section IV. As the LasDamas simulations assume a flat ΛCDM model with $\Omega_m = 0.25$ and $h = 0.7$, we adopt the same cosmology for the mocks.

2. *NYU-VAGC mock catalogs*

Starting directly from the previously described NYU-VAGC dataset, we generate a second set of mock catalogs built from the angular positions and spectroscopic redshifts of the observed galaxies. The goal of these mocks is to investigate the impact of known observational biases, incompleteness, and cosmic variance while preserving the spatial distributions of the galaxies in the real SDSS DR7 catalog.

---

[5] `http://lss.phy.vanderbilt.edu/lasdamas/mocks.html`

[6] Although the redshifts listed in the LasDamas `gamma` mocks include distortions from peculiar velocities, we interpret them as cosmological redshifts z_c for simplicity. This has no adverse effect on testing our method's performance.

TABLE I. Summary of the ΛCDM cosmologies described in the text.

Parameter set	Ω_b	Ω_m	Ω_Λ	h	n_s	σ_8
`param_mock`	0.0455	0.272	0.728	0.702	0.961	0.8
`param_wmap`	0.0442	0.2643	0.7357	0.714	0.969	0.814
`param_planck`	0.049	0.3175	0.6825	0.671	0.962	0.834

Just as in the case of the LasDamas mock catalogs, we interpret the observed spectroscopic redshifts as the cosmological ones and obtain the corresponding measured redshifts from eq. (14), where V is now determined from the full linear velocity field evaluated at redshift $z = 0$. The velocity field is obtained from a random realization sampled on a cubic grid with 1024^3 points and a comoving mesh size of $4h^{-1}$ Gpc, assuming the linear power spectrum $P_v(k)$ of a flat ΛCDM cosmology with total matter and baryonic density parameters $\Omega_m = 0.272$ and $\Omega_b = 0.0455$, respectively, scalar spectral index $n_s = 0.961$, $h = 0.702$, and $\sigma_8 = 0.8$ (corresponding to the parameter set `param_mock` which is listed in table I). To ensure a high level of (statistical) independence between the final mocks, we perform appropriate translations and rotations of the survey data reference frame relative to the sampling grid before each galaxy is assigned a velocity equal to that of the nearest grid point. Because of small-scale nonlinearities and the finite grid sampling, we further add uncertainties to the line-of-sight components of these velocities which are generated from a normal distribution with $\sigma_V = 250$ km s^{-1}.

The luminosities are assigned exactly as for the LasDamas mocks using the appropriate cuts in apparent and absolute magnitudes specified in section III A. In addition, we simulate two known systematic errors in the photometric calibration of SDSS data [57] that have a potential impact on our analysis. The first one arises from various magnitude offsets between the individual SDSS stripes, and is modeled by considering another random error with $\sigma_{\rm stripe} = 0.01$. The second, more serious error results from unmodeled atmospheric variations during the time of observation, ultimately causing an overall zero-point photometric tilt of roughly 0.01 in magnitudes over the survey region. To mimic this tilt, we include in each mock a magnitude offset in the form of a randomly oriented dipole normalized such that its associated root mean square (rms) over all galaxies is $\delta m_{\rm dipole} = 0.01$ [57].

With this procedure we obtain a total of 269 galaxy mocks (both flux- and volume-limited), mimicking the characteristics of the real NYU-VAGC sample. These mocks will be used to explore the distribution of measured bulk flow vectors and to study constraints on the power spectrum C_l or cosmological parameters for a realistic choice of the large-scale peculiar velocity field.

IV. DATA ANALYSIS

We now proceed to apply our method to the SDSS data. To achieve our goals outlined in section I, we will begin with a short description of some additional preliminaries and present the general line of action in section IV A. After this, we will estimate the r-band LF of SDSS galaxies at $z \sim 0.1$ in section IV B, which provides the basis for our investigations. The results of our velocity analysis of the NYU-VAGC galaxy sample are then presented and discussed in sections IV C and IV D.

A. General line of action

A major obstacle in constraining the velocity field from the SDSS is the partial coverage (only about 20%) of the sky. Since the Y_{lm} no longer form an orthogonal basis on this limited mask, the maximum-likelihood approach yields a statistical mixing between the estimated velocity moments, effectively probing a combination of different multipoles. In the case of the bulk flow, for instance, this would correspond to a superposition of several terms up to even the hexadecapole of the peculiar velocity field [58]. Of course, one may resort to an orthogonal basis set for $l_{\rm max}$ in pixel space. Because we are going through the full maximum-likelihood procedure, however, there is no gain in doing so, i.e. all the information is already contained in the measured a_{lm} and their covariance matrix. Also, the results expressed in such orthogonal bases typically have a less obvious physical interpretation.

Additional difficulties arise from a too flexible LF model, i.e. oversampling issues related to the spline-based estimator, and the linear evolution term $Q(z)$ which actually mimics the formally ignored monopole contribution in eq. (3) over the redshift range of interest. Both may contribute to the mode mixing and further complicate the interpretation of the corresponding results. Similarly, the presence of systematic errors in the SDSS photometry (see section III B) can lead to spurious flows which contaminate the velocity measurements and bias possible estimates of velocity power and cosmological parameters.

Despite these limitations, however, we show below that such measurements can still provide meaningful constraints if one interprets them with the help of suitable mock catalogs sharing the same angular mask (see section III B). For instance, estimates of different quantities

can be directly compared to the corresponding distributions obtained from the mocks where systematic effects are under control. As for the data (and mock) analysis presented below, we shall thus employ the following basic strategy:

(a) Assume a set of parameters that describe the background cosmology and select the galaxy sample according to the absolute magnitudes and luminosity distances computed, respectively, from apparent magnitudes and redshifts (see section III A).

(b) Assuming the linear luminosity evolution model specified in eq. (12), determine the $^{0.1}r$-band LF parameters including Q_0 for the case of a vanishing peculiar velocity field, i.e. $a_{lm} = 0$. The value of Q_0 is kept fixed in the following steps while the LF parameters are free to vary, except when using the fixed LF estimator explored in section IV C.

(c) Compute the maximum-likelihood estimate $\hat{\boldsymbol{x}}^{\mathrm{ML}}$ of the parameter vector $\boldsymbol{x}$ introduced in section II B for a suitable $l_{\max}$. These parameters specify both the velocity model and the LF. Approximating P_{tot} locally by a Gaussian distribution and taking the previously found ϕ with $a_{lm} = 0$ as an initial guess, this is achieved by iteratively solving for $\hat{\boldsymbol{x}}^{\mathrm{ML}}$ until the (exact) likelihood peak is reached. The required derivatives of $\log P_{\mathrm{tot}}$ can be calculated analytically and are summarized in appendix A. Convergence is reached after 3–5 iterations for a relative accuracy 10^{-6}–10^{-10}. The CPU time depends on the value of $l_{\max}$, but is typically around a few tens of minutes for about half a million objects. The results are potentially prone to mask-induced degeneracies related to the spline point separation ΔM when estimating the LF. We will describe below the various approaches used to investigate this issue.

(d) Estimate the random errors of $\hat{\boldsymbol{x}}^{\mathrm{ML}}$ from the covariance matrix $\boldsymbol{\Sigma}$ which is computed by directly inverting the observed Fisher matrix $\mathbf{F}$. The Fisher matrix $\mathbf{F}_{\alpha\beta} = -\partial \log P_{\mathrm{tot}}/(\partial x_\alpha \partial x_\beta)$ is evaluated at the maximum value $\hat{\boldsymbol{x}}^{\mathrm{ML}}$.[7]

(e) Marginalize the resulting distribution $P_{\mathrm{tot}}(\boldsymbol{d}|\boldsymbol{x})$ over all LF parameters that are unrelated to the velocity field and construct the posterior probability for the a_{lm} and, subsequently, the probability $P(C_l)$ according to the prescription given in section II B. Then maximize the latter with respect to C_l to estimate the angular power. Given the characteristics of the SDSS data, such estimates are expected to be quite uncertain, and thus we will limit ourselves to a proof of concept.

(f) Alternatively, consider a spatially flat ΛCDM model where the C_l are not free and independent, but fully determined by the cosmological parameters ζ_k, i.e. $C_l = C_l(\zeta_k)$. Constraints are obtained by sampling the probability $P[C_l(\zeta_k)]$ as a function of ζ_k on a discrete grid. Although other parameter choices are briefly discussed, we will focus on the quantity σ_8 which corresponds to the amplitude of the linear matter power spectrum on a scale of $8h^{-1}$ Mpc. To ensure that linear theory remains a valid description on the physical scales probed in the analysis, we further have to set $l_{\max}$ accordingly (see section IV D for details).

Except in the case of examining the LasDamas mocks, which contain substantially less galaxies than the other samples (see section III B above) and cover a smaller redshift range, we will consider the peculiar velocity field in two redshift bins with $0.02 < z_1 < 0.07 < z_2 < 0.22$, comprising about $N_1 \sim 1.5 \times 10^5$ and $N_2 \sim 3.5 \times 10^5$ galaxies, respectively. This specific choice is mainly driven by the accuracy of the bulk flow estimates presented in section IV C. For two redshift bins, the uncertainties are typically around 100 km s^{-1} which is also larger than the expected variation of the flow amplitude within the respective bins, yielding a good compromise between accuracy and evolution. Further, the actual bin widths are determined by requiring comparable signal-to-noise ratios which we roughly estimate from the expected variance of the velocity field within the corresponding bin volumes and the Poisson noise due the finite number of objects. As for the study of the observed data sample, we adopt the latest cosmological parameters based on the Wilkinson Microwave Anisotropy Probe (WMAP) combined with ground-based experiments [60] and the recent measurements by the Planck satellite [4] which are summarized in table I and denoted by `param_wmap` and `param_planck`, respectively.

B. The $^{0.1}r$-band luminosity function of NYU-VAGC galaxies

As described in section IV A, we begin with estimating $\phi(M)$ in the $^{0.1}r$-band from the NYU-VAGC data for a vanishing velocity field. Adopting the spline-based estimator with a separation of $\Delta M = 0.5$ between individual spline points, the resulting $\phi(M)$ is shown as a solid line in figure 1, where the normalization is chosen such that the integral of $\phi(M)$ over the considered absolute magnitude range becomes unity, i.e. $\eta(-22.5 + 5\log_{10} h, -17 + 5\log_{10} h) = 1$, and error bars are computed from the "constrained" covariance matrix obtained by enforcing the LF normalization to guarantee

[7] An immediate worry is that $\mathbf{F}$ could turn out singular or ill-conditioned. Except for issues, which are related to the normalization of the spline-based LF and can be easily overcome with the help of standard techniques [59], we have not encountered such problems in our study which considers only the first few multipoles, i.e. $l_{\max} \lesssim 5$.

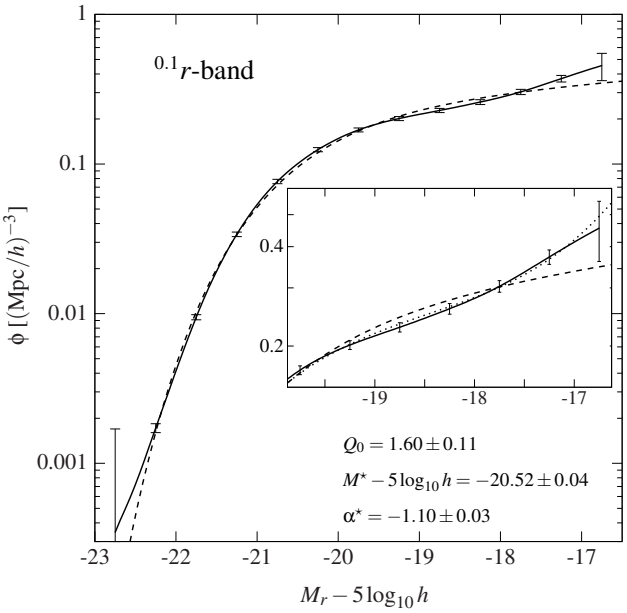

FIG. 1. The $^{0.1}r$-band LF as obtained from the NYU-VAGC sample: shown are the maximum-likelihood result adopting the spline-based estimator with $\Delta M = 0.5$ (solid line), and two fits based on the Schechter form (dashed line) and its extension (dotted line; zoomed panel only) which is defined by eq. (15).

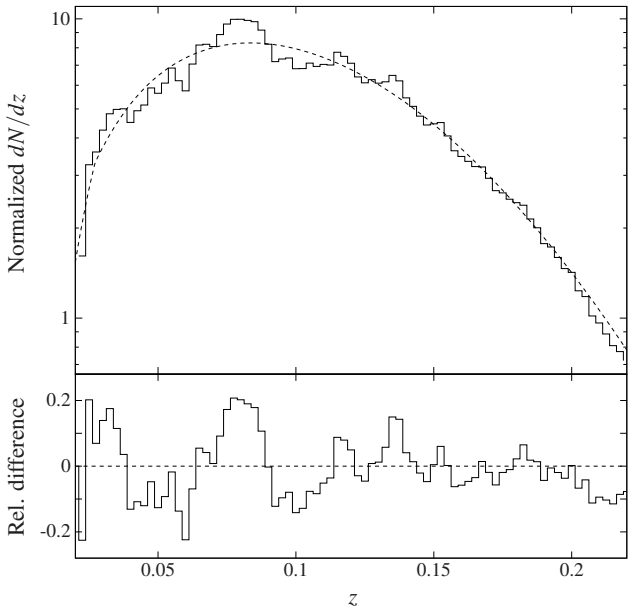

FIG. 2. Redshift distribution of SDSS galaxies from the NYU-VAGC sample: the histogram (solid line) represents the observed distribution normalized to unity over the considered redshift range for bins with $\Delta z = 2.5 \times 10^{-3}$. The predicted distribution (dashed line) assumes the spline-based estimate of the LF.

a non-singular Fisher matrix. The shape of $\phi(M)$ and the found evolution parameter, $Q_0 = 1.6 \pm 0.11$, are in good agreement with previous studies based on earlier data releases [56, 61]. While the simple Schechter form with $M^\star - 5\log_{10}h = -20.52 \pm 0.04$ and $\alpha^\star = -1.10 \pm 0.03$ (dashed line) describes the estimated ϕ reasonably well, it does not capture the visible feature at the faint end.[8] Therefore, we consider an extension to eq. (11) which, after using the relation $L/L^\star = 10^{0.4(M^\star - M)}$, takes the form

$$\phi \propto \left(\frac{L}{L^\star}\right)^{\beta_1^\star} \left[1 + 10^{-2.5}\left(\frac{L}{L^\star}\right)^{\beta_2^\star}\right] \exp\left(-\frac{L}{L^\star}\right) \quad (15)$$

and is equivalent to the sum of two Schechter functions with different choices of normalization and $\alpha^\star$. Fitting the above to the spline estimate yields the parameters $M^\star = -20.46 \pm 0.03$, $\beta_1^\star = -1.01 \pm 0.03$, and $\beta_2^\star = -1.64 \pm 0.11$, giving a much better representation of the observed trend. This is illustrated in the zoomed panel of figure 1, where the new result (dotted line) is compared to both the spline (solid line) and the previous Schechter fit (dashed line).

To further assess our result, we also calculate the predicted redshift distribution $\mathrm{d}N/\mathrm{d}z$ of galaxies which is directly proportional to the radial selection function $S(z)$, i.e. the fraction of galaxies included in the sample at redshift z. The selection function is easily obtained as an integral of the LF over the magnitude range defined by the redshift-dependent limiting absolute magnitudes. Figure 2 shows that the predicted and observed redshift distributions match quite well, except for a slight disagreement on the order of a few percent near the high-z cut. This small discrepancy is most likely caused by a combination of both the limited linear evolution model and the use of different K-corrections (individual and mean) when estimating $\phi(M)$ and the selection function (see section IV E for a discussion of how luminosity evolution and K-corrections impact our peculiar velocity results). Note that all of the above assumes the set `param_wmap`. Repeating the analysis with the parameters from `param_planck`, however, does not yield any significant changes.

[8] We emphasize that the variation in the faint-end slope is robust with respect to different choices of ΔM and not an artifact caused by the spline estimator.

C. Constraining bulk flows

As a first application of our method, we address how it may be used to constrain the bulk flow, $\boldsymbol{v}_B$, in the NYU-VAGC data. We begin with the LasDamas mocks for testing the ability of the method to detect large, anomalous bulk flows in a SDSS-like catalog. Then we apply the method to the real NYU-VAGC and discuss whether our results are consistent with the standard ΛCDM cosmology.

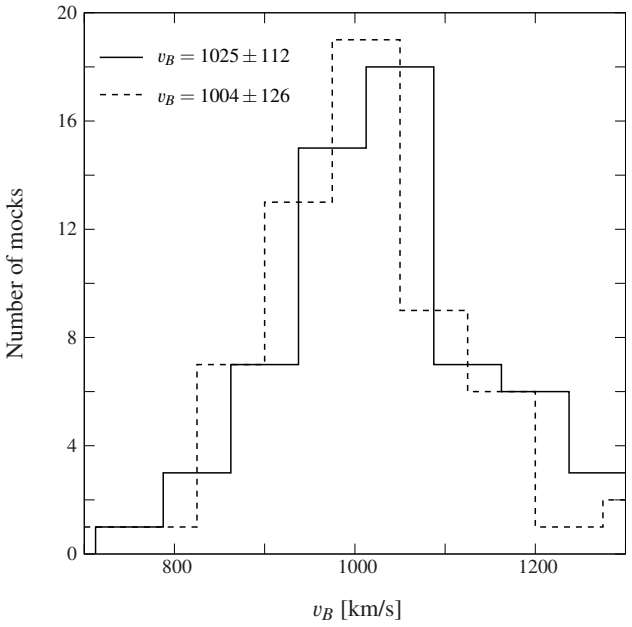

FIG. 3. Histograms of bulk flow measurements obtained from the customized LasDamas mocks: shown are the recovered distributions for both a known (dashed line) and unknown (solid line) flow direction.

1. LasDamas benchmark

We make use of the LasDamas mocks introduced in section III B and assume a constant $\boldsymbol{v}_B$ of 1000 km s^{-1} pointing toward the direction $(l, b) \approx (266°, 33°)$ expressed in Galactic coordinates. Note that both the magnitude and the direction of $\boldsymbol{v}_B$ are chosen in accordance with the recent controversial claim of a "dark flow" out to depths of around 300–600h^{-1} Mpc [19, 62–64].

Using the Schechter estimator for the LF and setting $l_{\max} = 1$, we follow the procedure outlined in section IV A to recover the flow $\boldsymbol{v}_B$ from the customized LasDamas mocks. The histogram in figure 3 shows the resulting component along the input direction for the cases that it is known (dashed line) and unknown (solid line), i.e. the direction is allowed to vary freely. Clearly, the magnitude of $\boldsymbol{v}_B$ is successfully extracted in both cases, and the corresponding rms values of 111 and 125 km s^{-1} are fully consistent with each other as is expected from Gaussian statistics. Although not presented here, the found distributions along the other (perpendicular) directions for a freely varying $\boldsymbol{v}_B$ are consistent with a zero velocity and exhibit a similar scatter. Of course, the current setup neglects any contamination due to leakage from other multipoles or systematic errors in the data. If these effects remain subdominant in the sense that their combination leads to changes comparable to or less than the estimated random errors, our result suggests that the method is capable of constraining large coherent bulk flows using the available galaxy data from the NYU-VAGC. As we will show below, this condition seems reasonably satisfied, at least for the results in the low-redshift bin with $0.02 < z < 0.07$.

2. Constraints from the NYU-VAGC

In the next step, we seek constraints on the velocity field for the case $l_{\max} = 1$, now using the real NYU-VAGC galaxy data. As we have argued above, the angular mask of our sample causes such "bulk flow" estimates to suffer from multipole mixing and their interpretation requires the use of mock catalogs. Another mask-related problem arises from additional degeneracies between the velocity multipoles and the LF, depending on the assumed spline point separation. For $\Delta M = 0.5$, this already becomes an issue, and the straightforward remedy is to increase the separation to an adequate value. To account for alternative solutions and to further judge our method's robustness, however, we will consider the following three representative approaches in our analysis:

(a) Fix the LF to its estimate for a vanishing velocity field, i.e. use a predetermined shape of $\phi(M)$ for the analysis. The rational of this fixed estimator is to evaluate the impact of adding degrees of freedom in the LF model.

(b) Adopt a hybrid model by fitting a Schechter form to the spline-based LF estimate for a vanishing velocity field and expressing the LF as the sum of a Schechter function and the corresponding (fixed) residual.

(c) Work exclusively with the Schechter parameterization of the LF.

Featuring the highest flexibility among the above, we expect estimates based on the hybrid LF model to be the most reliable ones. The corresponding flow measurements will be expressed in a specific Cartesian coordinate system defined by its x-, y-, and z-axes pointing toward Galactic coordinates $(l, b) \approx (81°, -7°)$, $(172°, -1°)$, and $(90°, 83°)$, respectively. In particular, the system's z-axis is chosen such that it approximately penetrates the central patch of galaxies observed in the northern hemisphere, and thus it is expected to give the tightest constraints. Using these coordinates, for example, the anomalous bulk flow incorporated in the LasDamas mocks (see the first paragraph of section IV C 1) can be written as $\boldsymbol{v}_B^{\mathrm{T}} \approx (-894, -80, 442)$ in units of km s^{-1}. To aid the following discussion of our results, let us further introduce v_K as the component along the direction of this anomalous flow which points toward $(l, b) \approx (266°, 33°)$.

Regarding the real NYU-VAGC galaxy sample, the inferred "bulk flows" for the cosmology defined by `param_wmap` are summarized in table II. A comparison between the estimated flow components shows that the results based on the various LF models are different, but consistent within their 1σ-values, where the quoted

TABLE II. Summary of "bulk flow" measurements ($l_{\max} = 1$) in two redshift bins for the parameter set `param_wmap` and the different models of the LF described in the text.

	$0.02 < z < 0.07$			$0.07 < z < 0.22$		
$\phi(M)$	v_x [km/s]	v_y [km/s]	v_z [km/s]	v_x [km/s]	v_y [km/s]	v_z [km/s]
Hybrid	-227 ± 128	-326 ± 113	-239 ± 73	-367 ± 92	-439 ± 85	-25 ± 71
Fixed	-175 ± 126	-278 ± 111	-147 ± 58	-340 ± 90	-409 ± 81	-45 ± 43
Schechter	-151 ± 130	-277 ± 116	-102 ± 78	-422 ± 93	-492 ± 86	-150 ± 74

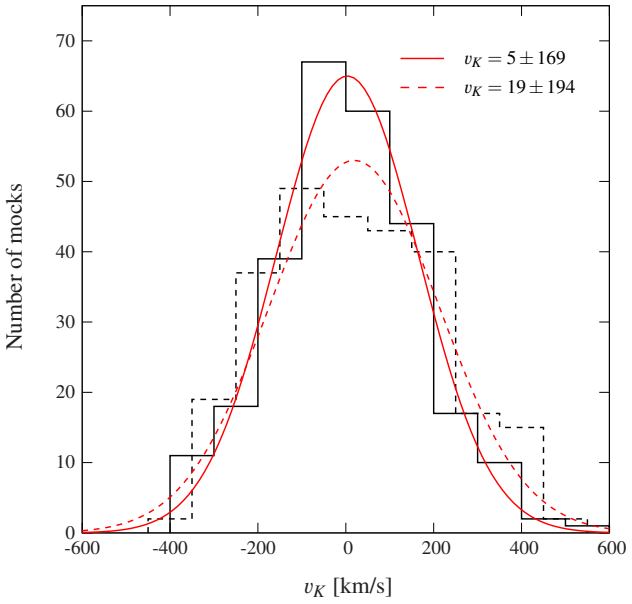

FIG. 4. Histograms of "bulk flow" measurements obtained from the simple NYU-VAGC mocks: shown are the recovered distributions (black lines) and corresponding Gaussian estimates (red lines) for the two redshift bins with $0.02 < z < 0.07$ (solid lines) and $0.07 < z < 0.22$ (dashed lines) along the direction of the anomalous flow assumed in the first paragraph of section IV C 1.

errors are derived from the observed Fisher information. All measurements are in very good agreement with $v_K \approx 120 \pm 115$ and 355 ± 80 km s^{-1} for the first and second redshift bin, respectively. To make sense of these numbers, we compare them to the distribution of v_K found with the help of the simple NYU-VAGC mocks (see section III B) which is presented in figure 4. Note that the mock analysis leading to this distribution has been performed using a pure Schechter estimator of the LF. Employing the other LF models listed above, however, gives very similar results and will leave our conclusions unchanged.[9] As can be seen from the figure, the observed distributions in both redshift bins are well described by Gaussian profiles with (nearly) zero mean and standard deviations of approximately 170 and 200 km s^{-1}, respectively. In contrast to the Fisher errors, the dispersion found from the mocks includes both the cosmic signal and contributions due to the magnitude dipole introduced in section III B. Repeating the mock analysis after removing the latter leads to a decrease in the dispersions of around 9% and 62% for the first and second bin, respectively. Systematic errors induced by the magnitude dipole are expected to increase with the redshift since a bulk flow with amplitude v_B is expected to induce a magnitude offset around $\delta m = 5 \log_{10}(1 - v_B/cz)$ [28]. On the contrary, cosmic variance is expected to decrease with the volume, and thus with the redshift. The increase of the dispersion with the redshift indicates that the errors induced by the magnitude dipole obliterate the contribution due to cosmic variance.

We find our measurements of v_K to be fully compatible with the distribution obtained from the mocks and consistent with zero at a 1σ (first redshift bin) and 2σ (second redshift bin) confidence level. Given that the estimated flow components are not necessarily uncorrelated, however, it is more appropriate to consider the joint distribution of the bulk flow components which is adequately characterized by a multivariate Gaussian. From our set of mocks and the actual data, we find that correlations between the different components are relatively mild and the corresponding (linear) correlation coefficients typically take values around 0.1–0.3. Choosing the hybrid model of the LF, for instance, the bulk flow measured in both bins is consistent with zero within 1.5σ if we adopt the usual confidence levels of multivariate normally distributed data with three degrees of freedom. Surprisingly, the bulk flow amplitudes associated with the estimated components in this case are $v_B \approx 490 \pm 100$ and 580 ± 80 expressed in units of km s^{-1}, where the errors are purely statistical and relatively small. Despite these rather large values, the recovered flows correspond to detections at the 1.5σ level. The reason is that the distribution of amplitudes does not follow a Gaussian, but has a long tail and is closely related to the χ^2-distribution. The estimated flows are pointing toward $(l, b) \approx (310°, -25°) \pm (30°, 10°)$ and $(310°, 5°) \pm (10°, 15°)$ in Galactic coordinates for the first and second redshift bin, respectively. Note that changing the cosmological parameters to `param_planck` or using the other LF models yields basically the same results.

[9] Despite having less degrees of freedom, this is also true in the case of the fixed LF estimator, where only the spread in the v_z-component is significantly reduced.

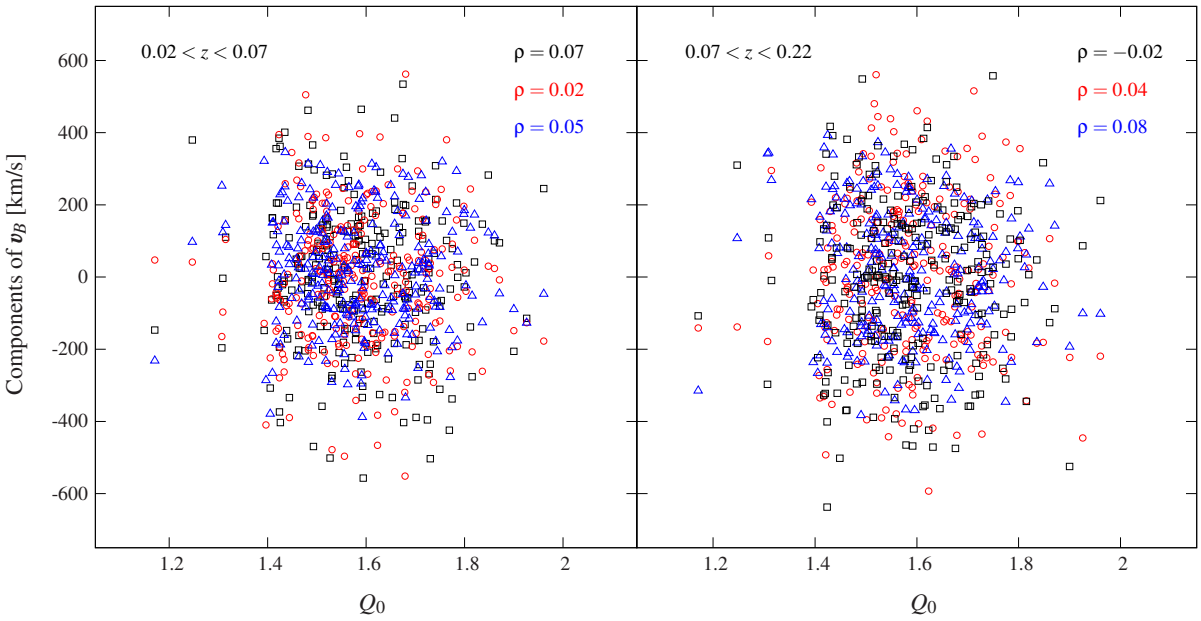

FIG. 5. Scatter plots of "bulk flow" components versus the linear evolution parameter Q_0 obtained from the simple NYU-VAGC mocks: the panels illustrate the resulting distributions of v_x (black squares), v_y (red circles), and v_z (blue triangles) for the two redshift bins with $0.02 < z < 0.07$ (left) and $0.07 < z < 0.22$ (right).

As for the comparison of our flow measurements with the mock catalog results, we point out that the simple NYU-VAGC mocks are not only built and analyzed with a slightly different cosmological model, but also ignore any redshift dependence of the peculiar velocity field which is assumed at $z = 0$ (see section III B). For typical choices of cosmological parameters and the redshift range of interest, this amounts to small differences $\lesssim 3\%$ and can, therefore, be ignored in our analysis. Another concern is that fixing the linear evolution as described in section IV A causes a bias in the flow components since the monopole-like term $Q(z)$ might leak in through the mask. To ensure that this is not the case, we plot the inferred components for both redshift bins against the estimate of the parameter Q_0 in figure 5. A brief visual inspection of the scatter already indicates that there is no evidence for a correlation between these quantities. This is confirmed by calculating the linear correlation coefficients which turn out smaller than 0.1 in all the cases. Together with the above findings, we thus conclude that the SDSS galaxy data exhibit no hint toward anomalously large flows. Accounting for the known magnitude tilt in the photometric calibration, our velocity measurements further appear fully consistent with the expectations of a ΛCDM cosmology.

D. Higher-order multipoles: constraining angular power and σ_8

As we have outlined in section II B, the luminosity-based approach considered in this work is analogous to the analysis of CMB anisotropies and, in principle, it is straightforward to constrain the angular velocity power spectrum using basically the same techniques. Given the characteristics of the SDSS data and our previous findings from section IV C, however, we already expect such constraints to be rather weak and potentially biased because of the systematic magnitude tilt described in section III B. Nevertheless, we shall explore the potential of this approach and illustrate some examples involving simple velocity models.

1. *Constraints with no cosmology priors*

Let us assume a velocity model with $l_{\rm max} = 2$ and assess the impact of a tilt in the zero-point photometry with the help of a mock galaxy catalog randomly chosen form the NYU-VAGC set. To facilitate a direct interpretation in terms of velocities, we additionally define the dimensional quantity

$$\tilde{C}_l \equiv \sqrt{\frac{2l+1}{4\pi} C_l} \tag{16}$$

which will be used in what follows below. Again, we assume the latest pre-Planck ΛCDM cosmology determined by `param_wmap` and also work with the hybrid estimator of the LF (see section IV C). Figure 6 shows the joint 1σ and 2σ confidence regions of $\tilde{C}_1$ and $\tilde{C}_2$, estimated after maximizing the likelihood $P(C_l)$ in eq. (8) for the same mock, with (right panel) and without (left panel) mimicking the systematic magnitude dipole offset (see section

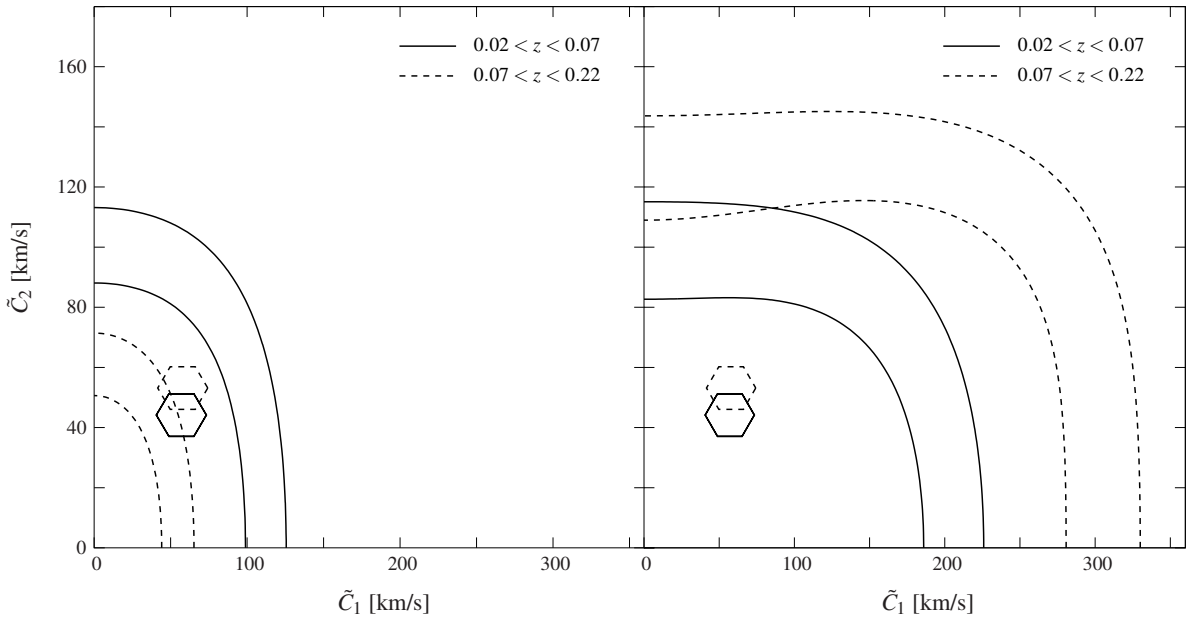

FIG. 6. Constraints on angular velocity power in a randomly selected mock for a model with $l_{\max} = 2$: shown are the joint 1σ and 2σ confidence regions of $\tilde{C}_1$ and $\tilde{C}_2$ (see text) for the first (solid lines) and second (dashed lines) redshift bin, respectively, estimated with (right panel) and without (left panel) a systematic dipole in the galaxy magnitudes. The hexagons indicate the corresponding results obtained from directly using the known galaxy velocities.

III B). Here the posterior likelihood is constructed separately for each redshift bin after marginalizing $P(\boldsymbol{d}|a_{lm})$ over the a_{lm} of the respective other one, and the resulting contour lines are derived using the quadratic estimator presented in ref. [37]. The effect of a spurious magnitude dipole mostly affects the probability contour along the $\tilde{C}_1$-axis, i.e. the power in the dipole, and as expected, the amplitude of the effect increases with the redshift. To quantify the smearing introduced when one estimates velocities through luminosity variations, we further compare the contours with the values of $\tilde{C}_1$ and $\tilde{C}_2$ inferred directly from the galaxy peculiar velocities in the mocks (hexagons in the figure). The estimated constraints are consistent with these values within the (large) 1–2σ bounds.

Repeating the analysis for the real SDSS galaxies, we end up with the confidence regions depicted in the left panel of figure 7. Although it is not very constraining in the present case, our analysis restricts the $\tilde{C}_l$ for $l_{\max} = 2$ to several hundred km s^{-1} and is consistent with zero power. This fully agrees with the predictions of the ΛCDM model and does not suggest any anomalous properties. We also note a striking resemblance in contour trends with the mock result in figure 6 from which it is tempting to deduce the existence of a formidable dipole contamination in the real data. Since, among other uncertainties, there is still leakage due to the survey geometry, however, strong statements like that cannot be made.

Including higher velocity multipoles with $l_{\max} \geq 3$, the constraints become even weaker as the level of degeneracy increases. To give a final example, we assume another model with fixed LF and set $l_{\max} = 3$. The corresponding confidence regions of the different $\tilde{C}_l$ are shown in right panel of figure 7. Note that the tighter bounds are only a consequence of reducing the available degrees of freedom.

2. Constraints with cosmology priors

Next, we shall consider constraints on cosmological parameters by imposing a ΛCDM prior on the angular power spectrum as detailed above in section II B. In doing so, it is convenient to divide the parameters that define the cosmological models into two categories. The ones that characterize the background cosmology and that are used to estimate absolute magnitudes and compute distances for sample selection, and those that characterize the density fluctuations. Here we focus on σ_8 which belongs to the latter category, and assume that all other parameters are fixed to their values in `param_wmap`. At the end of this section, we shall briefly discuss other choices and comment on the possibility of constraining background parameters such as Ω_m.

Like in the previous section, we assess the impact of a spurious tilt in the estimated magnitudes. To guarantee the validity of linear theory, we set $l_{\max} = 5$ which corresponds to considering physical scales above $\sim 100h^{-1}$ Mpc. Concerning the calculation of the theoretical C_l which is required for the prior probability and summarized in appendix C, we adopt the parameterized form of the matter power spectrum $P(k)$ given in ref. [65].

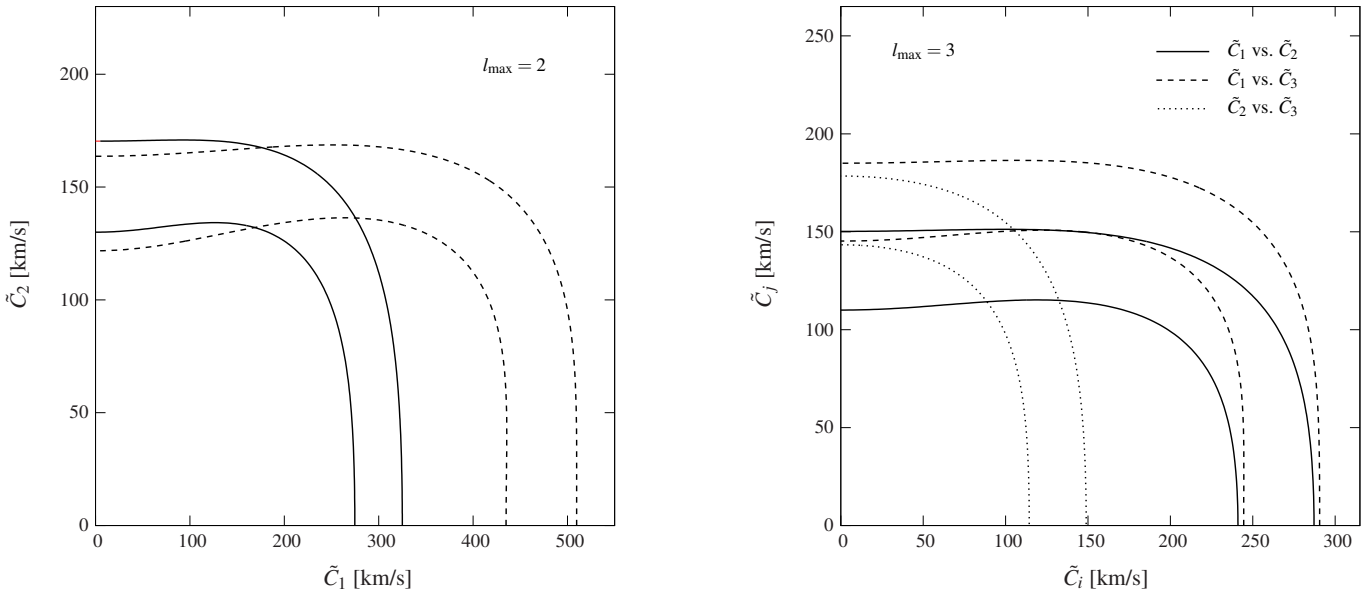

FIG. 7. Left panel: same as figure 6, but now for the real NYU-VAGC galaxy data which is missing direct velocity estimates. Right panel: adopting a model with $l_{\rm max} = 3$ and fixed LF to analyze the real galaxy data, the plot shows the marginalized joint 1σ and 2σ confidence regions of $\tilde{C}_1$ and $\tilde{C}_2$ (solid line), $\tilde{C}_1$ and $\tilde{C}_3$ (dashed line), and $\tilde{C}_2$ and $\tilde{C}_3$ (dotted line) for the first redshift bin.

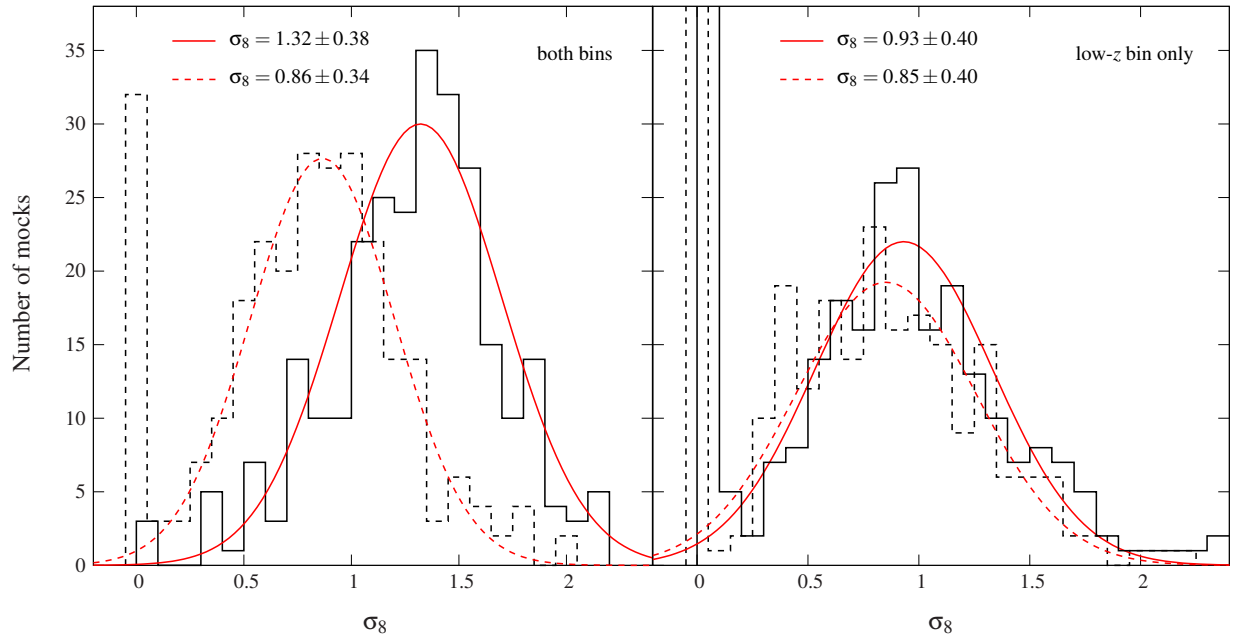

FIG. 8. Distribution of σ_8 estimated from the simple NYU-VAGC mocks: shown are the recovered histograms (black lines) with (solid lines) and without (dashed lines) the inclusion of a systematic dipole in the galaxy magnitudes, using the information in both redshift bins (left) and the first redshift bin with $0.02 < z < 0.07$ only (right). Note that the Gaussian curves (red lines) are obtained by fitting the observed cumulative distribution, excluding the cases where no large-scale power is detected.

Moreover, the galaxy redshift distribution $p(z)$ used to compute the bin-averaged velocity field given by eq. (C1) is taken to be of the form

$$p(z) \propto z^a \exp\left[-(z/\overline{z})^b\right], \qquad (17)$$

where the parameters $a = 1.31$, $b = 1.94$, and $\overline{z} = 0.1$ are found by directly fitting eq. (17) to the observed distribution. As is customary, σ_8 is inferred from discretely sampling the posterior probability and interpolating the corresponding result. In our calculations, we will choose

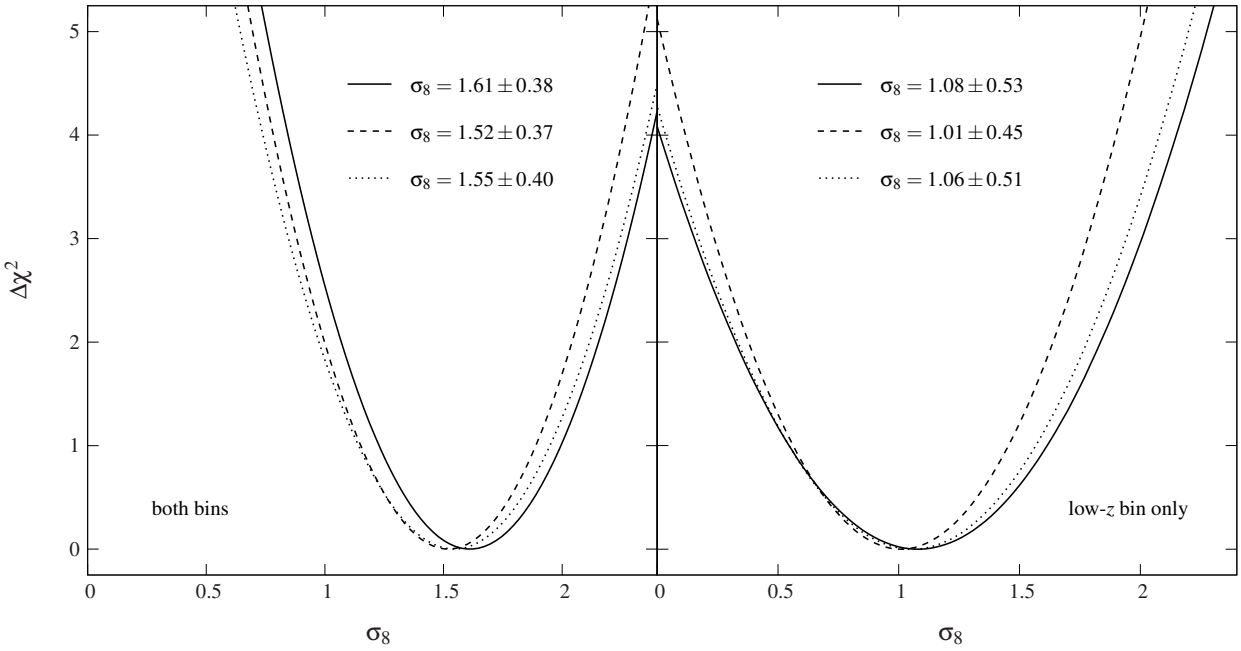

FIG. 9. Raw estimates of σ_8 obtained from the real NYU-VAGC galaxy data: shown is the derived $\Delta\chi^2$ as a function of σ_8 for both redshift bins (left panel) and the first redshift bin with $0.02 < z < 0.07$ only (right panel), adopting the hybrid (solid line), fixed (dashed line), and Schechter (dotted line) estimator of the LF.

a step size of 0.05.

Applying this procedure to the full suite of mock catalogs with and without the inclusion of a systematic magnitude dipole, we obtain the histograms shown in figure 8. While the results for the combination of both redshift bins stem from maximizing $P(C_l)$ in eq. (8) using the full probability $P(\boldsymbol{d}|a_{lm})$, those for the low-z bin are computed by constructing the posterior probability after marginalizing $P(\boldsymbol{d}|a_{lm})$ over all a_{lm} in the high-z bin. Note that the former approach is actually inconsistent as it incorrectly assumes that the a_{lm} are uncorrelated between different bins. Accounting for these missing correlations, however, leads only to differences of a few percent in the estimated values of σ_8 and its error, suggesting that they may be safely neglected. As described in section III B, the NYU-VAGC mocks are based on the parameter set `param_mock` and assume an input value of $\sigma_8 = 0.8$. In addition, we assume a Schechter LF for the mock analysis (just like in section IV C), but using the other LF models does not significantly change the results. The spikes in the histograms at $\sigma_8 = 0$ correspond to the cases in which we do not detect any power. Once we exclude those, the histograms are reasonably well represented by Gaussian distributions with standard deviations of ~ 0.3–0.4 (solid and dashed, red lines). As is readily seen from comparing the left and right panels, the presence of a systematic magnitude dipole (solid lines) causes a bias in the estimate of σ_8 which is rather severe for higher redshifts, i.e. $0.07 < z < 0.22$ (left panel). As expected, removing the dipole (dashed lines) also eliminates the bias, thus leading to the same mean value of σ_8 in both cases. Expressing the bias in numbers, the dipole contribution to galaxy magnitudes amounts to a systematic shift of $\Delta\sigma_8 \approx 0.13$ and $\Delta\sigma_8 \approx 0.52$ for the low-z bin and the combination of both redshift bins, respectively.

Considering now the real SDSS galaxy sample, we perform exactly the same analysis to obtain measurements of σ_8 for the different LF estimators introduced in section IV C. Our results are presented in figure 9 which shows the derived $\Delta\chi^2$ as a function of σ_8, obtained using the information from both redshift bins (left panel) and that of the first redshift bin only (right panel). Similar to what we have discovered in our investigation of "bulk flows", the values based on different LF models agree very well within their corresponding 1σ errors, and we get $\sigma_8 \sim 1.0$–1.1 in the low-z bin and $\sigma_8 \sim 1.5$–1.6 over the full z-range. Remarkably, the measured values and uncertainties closely match the inferred biased distributions of the previous mock analysis depicted in figure 8. If the magnitude tilt in the SDSS data is the only relevant source of systematic errors and sufficiently characterized by a dipole-like modulation, we can use the bias estimated from the mocks to correct our measurements. Taking the result of the hybrid LF estimator (solid line in figure 9), for example, we obtain corrected values of $\sigma_8 = 1.09 \pm 0.38$ (both bins) and $\sigma_8 = 0.95 \pm 0.53$ (low-z bin) which are fully compatible with each other and also consistent with the expectation of the ΛCDM model. The quoted errors are the statistical errors inferred from the NYU-VAGC data. Note that changing the cosmology to `param_planck` or choosing a different LF estimator has

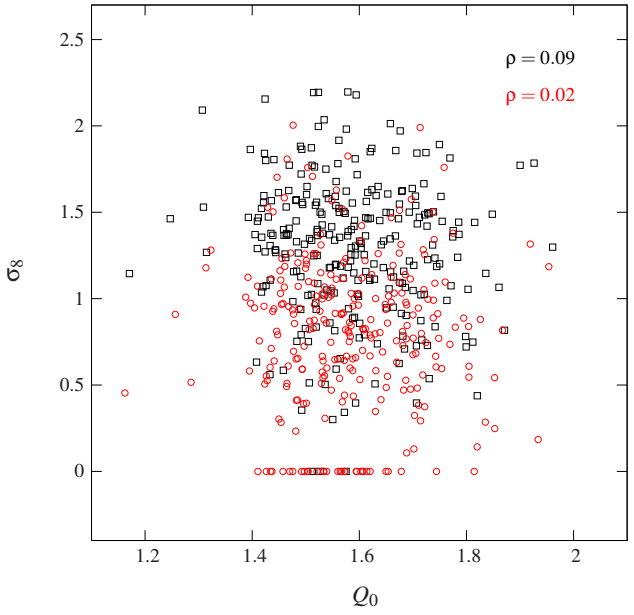

FIG. 10. Scatter plots of σ_8 versus the evolution parameter Q_0 for the simple NYU-VAGC mocks: using the information from both redshift bins, the plot illustrates the resulting distributions obtained with (black squares) and without (red circles) a systematic dipole in the galaxy magnitudes.

only a minor impact on the results.

Again, one may ask whether fixing the linear evolution as described in section IV A causes an additional bias in our measurements of σ_8. To answer this question, we plot the derived values of σ_8 for both redshift bins against the estimate of the evolution parameter Q_0 in figure 10, using the simple NYU-VAGC mocks with (black squares) and without (red circles) the magnitude dipole. As before (see section IV C), the linear correlation coefficients turn out $\lesssim 0.1$, and there is no indication for a correlation between these quantities.

Of course, one is not restricted to σ_8, but also free to look at other cosmological parameters or various combinations thereof. Considering the two parameters h and Ω_b which, together, determine the baryonic matter density, for instance, we find that the respective constraints turn out weaker than before, and are also highly degenerate with σ_8. Similar statements should hold for the parameter Ω_m. However, we do not explicitly check this because changing Ω_m alters the background cosmology and implies a modification of the survey volume and the selection of the galaxy sample. Taking this into account would substantially increase the workload of the analysis.

E. Caveats

1. *Coherent photometric errors and spurious signals*

Although our analysis of the SDSS galaxy data has tried to account for known systematics such as the zero-point photometric tilt (see the mock description in section III B), there could exist additional errors in the photometric calibration. It is important to note that the impact of such errors increases with the redshift and significantly affects the results obtained at $z \gtrsim 0.1$ in our analysis. An example is the possibility of zero-point offsets in magnitudes between the whole northern and southern hemispheres due to observing the galaxies in disconnected regions. If this offset was around 0.01–0.02, it should basically contribute a spurious flow of ~ 100–250 km s^{-1} to the actual bulk motion along the connecting axis, assuming a redshift of $z = 0.1$ for all galaxies. Since the SDSS footprint gives much more weight to the northern sample, however, the effect is much less pronounced. As we have verified with the help of our galaxy mocks, it has just a mild impact on velocity measurements along the previously defined z-axis (see section IV C), thus leaving our conclusions unchanged. In fact, the missing evidence for any large-scale flow anomaly found in sections IV C and IV D already indicates that there are no other relevant systematics which would otherwise require serious fine-tuning.

As for the photometric tilt, which constitutes the main source of systematic errors in the present analysis, it is worth pointing out that, although difficult in practice, such a photometric bias could in principle be characterized and corrected for by using additional information from star or galaxy counts and clustering from the very same SDSS DR7 dataset. Another possibility is to recalibrate the SDSS photometry with the help of independent datasets. For example, this could be accomplished using observations of the Panoramic Survey Telescope and Rapid Response System (Pan-STARRS) which covers 3/4 of the sky visible from Hawaii [66, 67] or, indeed, any future, wide galaxy survey with good photometric stability. With this respect, a major step forward in control on the photometric calibration is expected from galaxy surveys carried out from space like, for instance, the planned Euclid mission [68].

Imperfect corrections for Galactic extinction might also cause a systematic large-scale offset in the estimated magnitudes. In the NYU-VAGC, this correction is based on the maps given in ref. [46]. The recent comparison between these and the reddening maps obtained from the Pan-STARRS1 stellar photometry [69] does not hint at any large-scale coherent residual with an amplitude comparable to that of the known magnitude tilt. The new dust maps that will be obtained from the Planck data will settle the issue.

2. *Environmental dependence of the luminosity function*

There are several studies which strongly hint toward a dependence of the LF on the large-scale environment of galaxies [e.g., 70–75]. However, investigations trying to shed light on the connection between luminosity and galaxy density are typically limited to scales of a

few Mpc, thus not probing the large scales relevant to our work. As a matter of fact, an analysis addressing these environmental dependencies of galaxy luminosities on scales $\sim 100h^{-1}$ Mpc and above is still unavailable. Nonetheless, we may get an idea from extrapolating the observed dependence into the large-scale domain. Using that the rms of density fluctuations averaged over scales $\gtrsim 100h^{-1}$ is less than about 0.07, this gives rise to a particularly small effect if the overdensity of the large-scale environment turns out to be the most important factor. As we have already suggested in ref. [76], it should further be feasible to take such effects into account by performing measurements over independent volumes which are classified in terms of their average density.

3. *Luminosity evolution and K-corrections*

The analysis conducted in this paper assumes that the evolution of galaxy luminosity can be effectively described with a linear model of the form $Q(z) = Q_0(z-z_0)$ where $z_0 = 0.1$ and Q_0 is determined according to section IV A. To assess the robustness of our results with respect to this specific model, we have carried out a few simple tests. In a first run, we have examined the influence of varying Q_0 within its estimated 3σ confidence interval. This typically leads to changes in the measured "bulk flow" components of several tens of km s^{-1} and causes deviations less than 10% in the found values of σ_8. Moreover, we have explored nonlinear evolution models with second- and third-order terms. In this case, the corresponding changes in our velocity measurements turn out even smaller and can be safely neglected. Similarly, we have studied the impact of different K-corrections using the mean correction given by eq. (13) and two-dimensional polynomial fits as a function of redshift and $g-r$ color [77].[10] Again, the resulting differences are marginal and do not affect any of our conclusions.

V. CONCLUSIONS

We have exploited the well-known fact that peculiar motion induces spatially-coherent variations in the observed luminosity distribution of galaxies to probe the cosmic velocity field at $z \sim 0.1$ from the luminosity distribution of SDSS galaxies in the NYU-VAGC. The method adopted here extends the maximum-likelihood approach proposed in ref. [28] to constrain the peculiar velocity field beyond the bulk flow component. Considering the bin-averaged peculiar velocity field in two different redshift bins, $0.02 < z < 0.07$ and $0.07 < z < 0.22$, we have demonstrated how the method permits bounds on the corresponding angular velocity power spectrum and cosmological parameters. The main results of our analysis can be summarized as follows:

- To assess the robustness of our analysis against potential systematic errors, we have used a suite of mock galaxy catalogs obtained both from numerical simulations and from the NYU-VAGC dataset itself to match the real data as close as possible. We have identified three main obstacles which potentially hamper the analysis of the SDSS data: the survey geometry, which causes mixing between different moments, the possible degeneracies between the velocity multipoles and the estimator of the LF, and the presence of a coherent photometric tilt of about 0.01 magnitude across the survey region. While the impact of mode-to-mode mixing can be readily quantified by modeling the sky coverage and the influence of the LF has been evaluated by applying different estimators to the mocks, the latter effect is less trivial to account for. Here we have modeled the zero-point photometry offset by adding a randomly oriented dipole normalized such that the corresponding rms over all galaxies is $\delta m_{\rm dipole} = 0.01$ for each individual mock galaxy catalog. Our results suggest that the systematic tilt in the observed galaxy magnitudes is sufficiently described by this dipole contribution.

- Accounting for the known systematics in the SDSS photometry, the estimated "bulk flows" are consistent with the predictions of the standard ΛCDM model at $\lesssim 1$–2σ confidence in both redshift bins. The combined analysis of the corresponding three Cartesian components further corroborates this result. Using an independent estimator, this confirms the findings of the CMB studies in refs. [19, 21] which provide an upper bulk flow limit of a few hundred km s^{-1} at a 95% confidence limit on similar scales.

- Our analysis yields direct constraints on the angular velocity power spectrum C_l (considering terms up to the octupole) defined in section II B, independent of a prior on the cosmological model. All of the estimated C_l are consistent with the corresponding theoretical power spectra of the ΛCDM cosmology.

- Assuming a prior on the C_l as dictated by the ΛCDM model with fixed density parameters and a Hubble constant, we have used the method to infer the parameter σ_8 which determines the amplitude of the velocity field. After correcting for known systematics, we obtain $\sigma_8 \approx 1.1 \pm 0.4$ for the combination of both redshift bins and $\sigma_8 \approx 1.0 \pm 0.5$ for the low-redshift bin only. As anticipated, the found constraints on velocity moments and σ_8 are not very tight. However, they show the validity of

[10] As advised by the SDSS collaboration, we use model magnitudes to estimate the $g-r$ colors of galaxies.

our approach in view of future analyses with different datasets.

- As for the encountered data-inherent issues, current and next-generation spectroscopic surveys are designed to alleviate most of them, thanks to their large sky coverage (e.g., eBOSS[11], DESI [78, 79]) and improved photometric calibration in ground-based surveys (e.g., PAN-STARRS [66, 67]) and especially in space-borne experiments like Euclid [68]. Note that since uncertainties in the measured redshifts play a little role in our error budgets, the method is also suitable for application to wide photometric redshift surveys such as the 2MASS Photometric Redshift catalog (2MPZ) [80] and, again, Euclid.

- These excellent observational perspectives give us confidence that the method considered here will become a full-fledged cosmological probe, independent and alternative to the more traditional ones based on galaxy clustering, gravitational lensing and redshift space distortions. We expect that combining all these approaches will result in superior control over potential systematic errors that might affect the estimate of cosmological quantities, chief among them the growth rate $f(\Omega)$ of density fluctuations [31].

- The main interest here is the methodological aspect since the novel approach to estimate the angular velocity power spectrum or cosmological parameters, developed in analogy to the statistical treatment of CMB anisotropies, is to be regarded as a proof of concept guiding future analyses. As a final remark, we point out that it should be conceivable to reverse the ansatz taken in this work, allowing one to constrain luminosity evolution and to improve the photometric calibration of a galaxy sample in a given cosmological framework.

ACKNOWLEDGMENTS

This research was supported by the I-CORE Program of the Planning and Budgeting Committee, THE ISRAEL SCIENCE FOUNDATION (grants No. 1829/12 and No. 203/09), the German-Israeli Foundation for Research and Development, the Asher Space Research Institute, and in part by the Lady Davis Foundation. M.F. is supported by a fellowship from the Minerva Foundation. E.B. is supported by INFN-PD51 INDARK, MIUR PRIN 2011 "The dark Universe and the cosmic evolution of baryons: from current surveys to Euclid", and the Agenzia Spaziale Italiana from the agreement ASI/INAF/I/023/12/0.

Appendix A: Quadratic approximation of $\log P_{\rm tot}$

As previously discussed in section II B, the total log-likelihood of observing galaxies with absolute magnitudes M_i given their redshifts and radial peculiar velocities in a real (or simulated) dataset is

$$\log P_{\rm tot} = \sum_i \log P_i\left(M_i|z_i,V_i\right) = \sum_i \log \frac{\phi(M_i)}{\eta\left(M_i^+,M_i^-\right)}, \tag{A1}$$

where the function $\eta\left(M_i^+,M_i^-\right)$ and the limiting magnitudes $M_i^\pm$ are defined through eqs. (5) and (6). Assuming a set of LF and evolution parameters q_j as well as a redshift-binned velocity model $\tilde{V}(\hat{\boldsymbol{r}}) = \sum a_{lm} Y^*_{lm}(\hat{\boldsymbol{r}})$, we now seek an expansion of the form

$$\log P_i \approx \log P_i|_{\boldsymbol{x}=\boldsymbol{x}_0} + \sum_\alpha \left.\frac{\partial \log P_i}{\partial x_\alpha}\right|_{\boldsymbol{x}=\boldsymbol{x}_0} x_\alpha + \sum_{\alpha,\beta} \left.\frac{\partial^2 \log P_i}{\partial x_\alpha \partial x_\beta}\right|_{\boldsymbol{x}=\boldsymbol{x}_0} x_\alpha x_\beta. \tag{A2}$$

Here we have introduced $\boldsymbol{x}^{\rm T} = (q_j, a_{lm})$ and $\boldsymbol{x}_0$ corresponds to an arbitrary fixed parameter vector. Given a model of $\phi(M)$, it is then straightforward (but tedious) to derive the specific form of the above expansion by using eqs. (4–6) and the relations

$$\begin{aligned}
\frac{\partial {\rm DM}(z_c)}{\partial a_{lm}} &= -\frac{1+z}{c}\left.\frac{\partial {\rm DM}(z)}{\partial z}\right|_{z=z_c} Y^*_{lm} \\
\frac{\partial^2 {\rm DM}(z_c)}{\partial a_{lm}\partial a_{l'm'}} &= \left(\frac{1+z}{c}\right)^2 \left.\frac{\partial^2 {\rm DM}(z)}{\partial z^2}\right|_{z=z_c} Y^*_{lm} Y^*_{l'm'},
\end{aligned} \tag{A3}$$

where the Y_{lm} are evaluated at the position of the galaxy in question. In the following, we shall give some details regarding the calculation for the two models of $\phi(M)$ adopted in our analysis.

[11] http://www.sdss3.org/future/

1. Schechter form

Assuming a Schechter LF, we start from [43]

$$\phi(M) = 0.4\log(10)\phi^\star 10^{0.4(1+\alpha^\star)(M^\star - M)} \exp\left(-10^{0.4(M^\star - M)}\right), \tag{A4}$$

with the usual Schechter parameters given as $M^\star$, $\alpha^\star$, and $\phi^\star$. The only non-trivial derivatives appearing in eq. (A2) are those of $\eta\left(M^+, M^-\right)$ with respect to $\alpha^\star$. Since eq. (5) can be written in terms of the incomplete gamma function, i.e.

$$\eta\left(M^+, M^-\right) = \phi^\star\left[\Gamma\left(1+\alpha^\star, \tilde{L}^-\right) - \Gamma\left(1+\alpha^\star, \tilde{L}^+\right)\right], \tag{A5}$$

the corresponding expressions can be obtained with the help of

$$\begin{aligned}
\frac{\partial\Gamma\left(1+\alpha^\star, \tilde{L}\right)}{\partial\alpha^\star} &= \Gamma\left(1+\alpha^\star, \tilde{L}\right)\log\tilde{L} + \mathcal{A}\left(\alpha^\star, \tilde{L}\right), \\
\frac{\partial^2\Gamma\left(1+\alpha^\star, \tilde{L}\right)}{\partial\alpha^{\star 2}} &= \left[\Gamma\left(1+\alpha^\star, \tilde{L}\right)\log\tilde{L} + 2\mathcal{A}\left(\alpha^\star, \tilde{L}\right)\right]\log\tilde{L} + \mathcal{B}\left(\alpha^\star, \tilde{L}\right),
\end{aligned} \tag{A6}$$

where $\tilde{L} = L/L^\star = 10^{0.4(M^\star - M)}$,

$$\begin{aligned}
\mathcal{A} &= \frac{\psi^{(0)}(1+\alpha^\star) - \log\tilde{L}}{\Gamma(-\alpha^\star)\sin\left[\pi(1+\alpha^\star)\right]}\pi + \tilde{L}^{1+\alpha^\star}\sum_{n=0}^{\infty}\frac{(-1)^n\tilde{L}^n}{n!(1+\alpha^\star+n)^2}, \\
\mathcal{B} &= \frac{\psi^{(1)}(1+\alpha^\star) + \left(\psi^{(0)}(1+\alpha^\star) - \log\tilde{L}\right)^2}{\Gamma(-\alpha^\star)\sin\left[\pi(1+\alpha^\star)\right]}\pi - 2\tilde{L}^{1+\alpha^\star}\sum_{n=0}^{\infty}\frac{(-1)^n\tilde{L}^n}{n!(1+\alpha^\star+n)^3},
\end{aligned} \tag{A7}$$

and $\psi^{(s)}$ denotes the polygamma function of degree s. Note that the above relations remain strictly valid only as long as $\tilde{L} < 1$ and $1+\alpha^\star$ is neither zero nor a negative integer.

2. Cubic spline

Choosing an equidistant set of sampling points (M_i, ϕ_i) with $0 \le i < N$, the LF may be modeled as a natural cubic spline with piecewise definition [41]

$$\phi(M) = (1-t_i)\phi_{i-1} + t_i\phi_i + t_i(1-t_i)\left[a_i(1-t_i) + b_i t_i\right], \qquad M_{i-1} \le M < M_i, \tag{A8}$$

where i now runs from 1 to $N-1$, $t_i = (M - M_i)/\Delta M$ and

$$a_i = k_{i-1}\Delta M - (\phi_i - \phi_{i-1}), \qquad b_i = -k_i\Delta M + (\phi_i - \phi_{i-1}). \tag{A9}$$

The k_i can be written in terms of an appropriate tridiagonal matrix A_{ij} whose inverse solves the spline problem, and introducing the Kronecker delta $\delta^K_{i,j}$, one has

$$k_i = \frac{3}{\Delta M^2}\sum_j A^{-1}_{ij}\left[\left(1-\delta^K_{0,j}\right)\left(\phi_j - \phi_{j-1}\right) + \left(1-\delta^K_{N-1,j}\right)\left(\phi_{j+1} - \phi_j\right)\right]. \tag{A10}$$

Since we are dealing with polynomials, evaluating the expansion in (A2) only requires basic calculus. To obtain the derivatives of a_i and b_i, for instance, one easily verifies that

$$\frac{\partial k_i}{\partial\phi_j} = \frac{3}{\Delta M^2}\left[\left(1-\delta^K_{0,j}\right)A^{-1}_{i,j-1} + \left(\delta^K_{N-1,j} - \delta^K_{0,j}\right)A^{-1}_{i,j} - \left(1-\delta^K_{N-1,j}\right)A^{-1}_{i,j+1}\right]. \tag{A11}$$

Similarly, piecewise integration of eq. (A8) yields

$$\begin{aligned}
\frac{1}{\Delta M}\int\phi(M')\mathrm{d}M' = &\left(t_i - \frac{1}{2}t_i^2\right)\phi_{i-1} + \frac{1}{2}t_i^2\phi_i + a_i\left(\frac{1}{2} - \frac{2}{3}t_i + \frac{1}{4}t_i^2\right)t_i^2 \\
&+ b_i\left(\frac{1}{3} - \frac{1}{4}t_i\right)t_i^3, \qquad M_{i-1} \le M' < M_i,
\end{aligned} \tag{A12}$$

which may be used to compute certain derivatives of $\eta\left(M^+, M^-\right)$. Note that because of the spline equation's linearity, all second derivatives with respect to the spline parameters ϕ_j trivially vanish.

Appendix B: Constructing the probability $P(C_l)$ for Gaussian fields

Starting from Bayes' theorem, we write the posterior probability as

$$P(a_{lm}|\boldsymbol{d}) \propto P\left(\boldsymbol{d}|a_{lm}\right) P\left(a_{lm}|C_l\right). \tag{B1}$$

Assuming that the probabilities $P(\boldsymbol{d}|a_{lm})$ and $P(a_{lm}|C_l)$ correspond to Gaussian distributions $\mathcal{N}(\boldsymbol{a}, \boldsymbol{\Sigma}_M)$ and $\mathcal{N}(0, \mathbf{D})$, respectively, evaluating the integral in eq. (8) yields

$$\log P(C_l) = \log P\left(\boldsymbol{d}|C_l\right) = -\frac{1}{2}\left[\boldsymbol{a}^{\mathrm{T}}\mathbf{Q}^{-1}\boldsymbol{a} + \mathrm{Tr}\left(\log \mathbf{Q}\right)\right] + \mathrm{const}, \tag{B2}$$

where $\boldsymbol{\Sigma}_M$ denotes the marginal covariance matrix constructed from the original one (i.e. the full matrix $\boldsymbol{\Sigma}$ which has been introduced in section II B), $\mathbf{D}$ is a diagonal matrix which depends on the C_l, and $\mathbf{Q} = \boldsymbol{\Sigma}_M + \mathbf{D}$ is assumed to be non-singular. Analog to the analysis of CMB anisotropies, the power spectrum is now estimated by maximizing the probability in eq. (B2) with respect to the C_l. To obtain an error for this estimate, we simply expand the logarithm of $P(C_l)$ around the maximum (assumed as well-defined) to quadratic order and compute the inverse of the corresponding curvature matrix. One may easily verify that the required derivatives with respect to C_l are explicitly given by

$$\frac{\partial \log P(C_l)}{\partial C_l} = \frac{1}{2}\left[\boldsymbol{a}^{\mathrm{T}}\mathbf{Q}^{-1}\frac{\partial \mathbf{D}}{\partial C_l}\mathbf{Q}^{-1}\boldsymbol{a} - \mathrm{Tr}\left(\mathbf{Q}^{-1}\frac{\partial \mathbf{D}}{\partial C_l}\right)\right] \tag{B3}$$

and

$$\frac{\partial^2 \log P}{\partial C_l \partial C_{l'}} = -\boldsymbol{a}^{\mathrm{T}}\mathbf{Q}^{-1}\frac{\partial \mathbf{D}}{\partial C_l}\mathbf{Q}^{-1}\frac{\partial \mathbf{D}}{\partial C_{l'}}\mathbf{Q}^{-1}\boldsymbol{a} + \frac{1}{2}\,\mathrm{Tr}\left(\mathbf{Q}^{-1}\frac{\partial \mathbf{D}}{\partial C_l}\mathbf{Q}^{-1}\frac{\partial \mathbf{D}}{\partial C_{l'}}\right). \tag{B4}$$

Using that $\langle \boldsymbol{a}\boldsymbol{a}^{\mathrm{T}}\rangle = \mathbf{Q}$, it further follows that

$$\left\langle \frac{\partial^2 \log P}{\partial C_l \partial C_{l'}} \right\rangle = -\frac{1}{2}\,\mathrm{Tr}\left(\mathbf{Q}^{-1}\frac{\partial \mathbf{D}}{\partial C_l}\mathbf{Q}^{-1}\frac{\partial \mathbf{D}}{\partial C_{l'}}\right). \tag{B5}$$

Appendix C: Theoretical C_l for the ΛCDM cosmology

In what follows, we will present predictions for the angular power spectrum of the peculiar velocity field introduced in section II for the standard ΛCDM cosmology. Since the observed galaxies are divided into redshift bins, we consider the averaged velocity field

$$\tilde{V}(\hat{\boldsymbol{r}}) = \int_{r_1}^{r_2} V\left[\hat{\boldsymbol{r}}r, t(r)\right] p(r)\mathrm{d}r. \tag{C1}$$

Here r_1 and r_2 are the comoving distances at the limiting redshifts of a given bin, and $p(r)dr$ is the probability of observing a galaxy within the interval $[r, r+dr]$. We thus begin with

$$a_{lm} = \int \mathrm{d}\Omega \tilde{V}(\hat{\boldsymbol{r}}) Y_{lm}(\hat{\boldsymbol{r}}) = -\int \mathrm{d}\Omega Y_{lm}(\hat{\boldsymbol{r}}) \int_{r_1}^{r_2} W(r)\frac{\partial \Phi_0(\hat{\boldsymbol{r}}r)}{\partial r}\mathrm{d}r, \tag{C2}$$

where we have used $\tilde{V}(\hat{\boldsymbol{r}}) = \sum a_{lm} Y^*_{lm}(\hat{\boldsymbol{r}})$, the definition $W(r) = 2a\dot{D}p(r)/3\Omega_0 H_0^2$, and the linear relation

$$V(\boldsymbol{r}, t) = -\frac{2}{3}\frac{a\dot{D}(t)}{\Omega_0 H_0^2}\frac{\partial \Phi_0}{\partial r}, \tag{C3}$$

with $D(t)$ and $a(t)$ evaluated at $t = t(r)$. Expanding $\Phi_0(\boldsymbol{r})$ in Fourier space, i.e.

$$\Phi_0(\boldsymbol{r}) = \frac{1}{(2\pi)^3}\int \mathrm{d}^3k \Phi_{\boldsymbol{k}} \mathrm{e}^{\mathrm{i}\boldsymbol{k}\cdot\boldsymbol{r}}, \tag{C4}$$

and exploiting the plane wave expansion

$$\mathrm{e}^{\mathrm{i}\boldsymbol{k}\cdot\boldsymbol{r}} = 4\pi \sum_{l,m} \mathrm{i}^l j_l(kr) Y^*_{lm}(\hat{\boldsymbol{r}}) Y_{lm}(\hat{\boldsymbol{k}}), \tag{C5}$$

where j_l are the usual spherical Bessel functions of the first kind, we get

$$a_{lm} = -\frac{\mathrm{i}^l}{2\pi^2}\int_{r_1}^{r_2}\mathrm{d}rW(r)\int\mathrm{d}^3k\Phi_{\boldsymbol{k}}\left(\frac{lj_l}{r}-kj_{l+1}\right)Y_{lm}(\hat{\boldsymbol{k}}). \tag{C6}$$

Therefore, using that $\langle\Phi_{\boldsymbol{k}}\Phi_{\boldsymbol{k}'}\rangle = (2\pi)^3\delta_D(\boldsymbol{k}-\boldsymbol{k}')P_\Phi(k)$, we finally arrive at

$$C_l = \left\langle|a_{lm}|^2\right\rangle = \frac{2}{\pi}\int\mathrm{d}kk^2P_\Phi(k)\left|\int_{r_1}^{r_2}\mathrm{d}rW(r)\left(\frac{lj_l}{r}-kj_{l+1}\right)\right|^2. \tag{C7}$$

[1] W. J. Percival, B. A. Reid, D. J. Eisenstein, N. A. Bahcall, T. Budavari, J. A. Frieman, M. Fukugita, J. E. Gunn, Ž. Ivezić, G. R. Knapp, and et al., MNRAS, **401**, 2148 (2010), arXiv:0907.1660 [astro-ph.CO].

[2] A. G. Riess, L. Macri, S. Casertano, H. Lampeitl, H. C. Ferguson, A. V. Filippenko, S. W. Jha, W. Li, and R. Chornock, ApJ, **730**, 119 (2011), arXiv:1103.2976 [astro-ph.CO].

[3] G. Hinshaw, D. Larson, E. Komatsu, D. N. Spergel, C. L. Bennett, J. Dunkley, M. R. Nolta, M. Halpern, R. S. Hill, N. Odegard, and et al., ApJ. S, **208**, 19 (2013), arXiv:1212.5226 [astro-ph.CO].

[4] Planck Collaboration, P. A. R. Ade, N. Aghanim, C. Armitage-Caplan, M. Arnaud, M. Ashdown, F. Atrio-Barandela, J. Aumont, C. Baccigalupi, A. J. Banday, and et al., ArXiv e-prints (2013), arXiv:1303.5076 [astro-ph.CO].

[5] A. G. Riess, W. H. Press, and R. P. Kirshner, ApJL, **445**, L91 (1995), astro-ph/9412017.

[6] A. Dekel, A. Eldar, T. Kolatt, A. Yahil, J. A. Willick, S. M. Faber, S. Courteau, and D. Burstein, ApJ, **522**, 1 (1999), astro-ph/9812197.

[7] S. Zaroubi, M. Bernardi, L. N. da Costa, Y. Hoffman, M. V. Alonso, G. Wegner, C. N. A. Willmer, and P. S. Pellegrini, MNRAS, **326**, 375 (2001), astro-ph/0005558.

[8] M. J. Hudson, R. J. Smith, J. R. Lucey, and E. Branchini, MNRAS, **352**, 61 (2004), astro-ph/0404386.

[9] D. Sarkar, H. A. Feldman, and R. Watkins, MNRAS, **375**, 691 (2007), astro-ph/0607426.

[10] G. Lavaux, R. B. Tully, R. Mohayaee, and S. Colombi, ApJ, **709**, 483 (2010), arXiv:0810.3658.

[11] H. A. Feldman, R. Watkins, and M. J. Hudson, MNRAS, **407**, 2328 (2010), arXiv:0911.5516 [astro-ph.CO].

[12] A. Nusser and M. Davis, ApJ, **736**, 93 (2011), arXiv:1101.1650 [astro-ph.CO].

[13] S. J. Turnbull, M. J. Hudson, H. A. Feldman, M. Hicken, R. P. Kirshner, and R. Watkins, MNRAS, **420**, 447 (2012), arXiv:1111.0631 [astro-ph.CO].

[14] U. Feindt, M. Kerschhaggl, M. Kowalski, G. Aldering, P. Antilogus, C. Aragon, S. Bailey, C. Baltay, S. Bongard, C. Buton, and et al., A&A, **560**, A90 (2013), arXiv:1310.4184 [astro-ph.CO].

[15] R. B. Tully and J. R. Fisher, A&A, **54**, 661 (1977).

[16] D. Lynden-Bell, S. M. Faber, D. Burstein, R. L. Davies, A. Dressler, R. J. Terlevich, and G. Wegner, ApJ, **326**, 19 (1988).

[17] M. A. Strauss and J. A. Willick, Physics Reports, **261**, 271 (1995), astro-ph/9502079.

[18] M. G. Haehnelt and M. Tegmark, MNRAS, **279**, 545 (1996), astro-ph/9507077.

[19] S. J. Osborne, D. S. Y. Mak, S. E. Church, and E. Pierpaoli, ApJ, **737**, 98 (2011), arXiv:1011.2781 [astro-ph.CO].

[20] G. Lavaux, N. Afshordi, and M. J. Hudson, MNRAS, **430**, 1617 (2013), arXiv:1207.1721 [astro-ph.CO].

[21] The Planck Collaboration, P. A. R. Ade, N. Aghanim, M. Arnaud, M. Ashdown, J. Aumont, C. Baccigalupi, A. Balbi, A. J. Banday, R. B. Barreiro, and et al., A&A, **561**, A97 (2014), arXiv:1303.5090.

[22] A. J. S. Hamilton, in *The Evolving Universe*, Astrophysics and Space Science Library, Vol. 231, edited by D. Hamilton (1998) p. 185.

[23] J. A. Peacock, S. Cole, P. Norberg, C. M. Baugh, J. Bland-Hawthorn, T. Bridges, R. D. Cannon, M. Colless, C. Collins, W. Couch, and et al., Nature, **410**, 169 (2001), astro-ph/0103143.

[24] R. Scoccimarro, Physical Review D., **70**, 083007 (2004), astro-ph/0407214.

[25] L. Guzzo, M. Pierleoni, B. Meneux, E. Branchini, O. Le Fèvre, C. Marinoni, B. Garilli, J. Blaizot, G. De Lucia, A. Pollo, and et al., Nature, **451**, 541 (2008), arXiv:0802.1944.

[26] G. A. Tammann, A. Yahil, and A. Sandage, ApJ, **234**, 775 (1979).

[27] J. P. Huchra, L. M. Macri, K. L. Masters, T. H. Jarrett, P. Berlind, M. Calkins, A. C. Crook, R. Cutri, P. Erdoğdu, E. Falco, and et al., ApJ. S, **199**, 26 (2012), arXiv:1108.0669 [astro-ph.CO].

[28] A. Nusser, E. Branchini, and M. Davis, ApJ, **735**, 77 (2011), arXiv:1102.4189 [astro-ph.CO].

[29] E. Branchini, M. Davis, and A. Nusser, MNRAS, **424**, 472 (2012), arXiv:1202.5206 [astro-ph.CO].

[30] A. Nusser and M. Davis, ApJL, **421**, L1 (1994), astro-ph/9309009.

[31] A. Nusser, E. Branchini, and M. Davis, ApJ, **744**, 193 (2012), arXiv:1106.6145 [astro-ph.CO].

[32] D. G. York, J. Adelman, J. E. Anderson, Jr., S. F. Anderson, J. Annis, N. A. Bahcall, J. A. Bakken, R. Barkhouser, S. Bastian, E. Berman, and SDSS Collaboration, AJ, **120**, 1579 (2000), astro-ph/0006396.

[33] D. J. Fixsen, E. S. Cheng, J. M. Gales, J. C. Mather, R. A. Shafer, and E. L. Wright, ApJ, **473**, 576 (1996), astro-ph/9605054.

[34] R. K. Sachs and A. M. Wolfe, ApJ, **147**, 73 (1967).

[35] M. R. Blanton and S. Roweis, AJ, **133**, 734 (2007), astro-ph/0606170.

[36] M. Tegmark, Physical Review D., **55**, 5895 (1997), astro-ph/9611174.

[37] J. R. Bond, A. H. Jaffe, and L. Knox, Physical Review D., **57**, 2117 (1998), astro-ph/9708203.

[38] Y. Itoh, K. Yahata, and M. Takada, Physical Review D., **82**, 043530 (2010), arXiv:0912.1460 [astro-ph.CO].

[39] A. Abate and H. A. Feldman, MNRAS, **419**, 3482 (2012), arXiv:1106.5791 [astro-ph.CO].

[40] G. Efstathiou, R. S. Ellis, and B. A. Peterson, MNRAS, **232**, 431 (1988).

[41] W. H. Press, S. A. Teukolsky, W. T. Vetterling, and B. P. Flannery, *Numerical recipes in C++ : the art of scientific computing by William H. Press. xxviii, 1,002 p. : ill. ; 26 cm. Includes bibliographical references and index. ISBN : 0521750334* (Cambridge University Press, 2nd ed., 2002).

[42] A. Sandage, G. A. Tammann, and A. Yahil, ApJ, **232**, 352 (1979).

[43] P. L. Schechter, Astronomical Journal, **85**, 801 (1980).

[44] M. R. Blanton, D. J. Schlegel, M. A. Strauss, J. Brinkmann, D. Finkbeiner, M. Fukugita, J. E. Gunn, D. W. Hogg, Ž. Ivezić, G. R. Knapp, and et al., AJ, **129**, 2562 (2005), astro-ph/0410166.

[45] K. N. Abazajian, J. K. Adelman-McCarthy, M. A. Agüeros, S. S. Allam, C. Allende Prieto, D. An, K. S. J. Anderson, S. F. Anderson, J. Annis, N. A. Bahcall, and et al., ApJ. S, **182**, 543 (2009), arXiv:0812.0649.

[46] D. J. Schlegel, D. P. Finkbeiner, and M. Davis, ApJ, **500**, 525 (1998), astro-ph/9710327.

[47] M. R. Blanton, J. Dalcanton, D. Eisenstein, J. Loveday, M. A. Strauss, M. SubbaRao, D. H. Weinberg, J. E. Anderson, Jr., J. Annis, N. A. Bahcall, and et al., AJ, **121**, 2358 (2001), astro-ph/0012085.

[48] M. A. Strauss, D. H. Weinberg, R. H. Lupton, V. K. Narayanan, J. Annis, M. Bernardi, M. Blanton, S. Burles, A. J. Connolly, J. Dalcanton, and et al., AJ, **124**, 1810 (2002), astro-ph/0206225.

[49] J. B. Oke and J. E. Gunn, ApJ, **266**, 713 (1983).

[50] D. J. Eisenstein, J. Liebert, H. C. Harris, S. J. Kleinman, A. Nitta, N. Silvestri, S. A. Anderson, J. C. Barentine, H. J. Brewington, J. Brinkmann, and et al., ApJ. S, **167**, 40 (2006), astro-ph/0606700.

[51] M. R. Blanton, J. Brinkmann, I. Csabai, M. Doi, D. Eisenstein, M. Fukugita, J. E. Gunn, D. W. Hogg, and D. J. Schlegel, AJ, **125**, 2348 (2003), astro-ph/0205243.

[52] C. McBride, A. Berlind, R. Scoccimarro, R. Wechsler, M. Busha, J. Gardner, and F. van den Bosch, in *American Astronomical Society Meeting Abstracts #213*, Bulletin of the American Astronomical Society, Vol. 41 (2009) p. 425.06.

[53] J. A. Peacock and R. E. Smith, MNRAS, **318**, 1144 (2000), astro-ph/0005010.

[54] U. Seljak, MNRAS, **318**, 203 (2000), astro-ph/0001493.

[55] A. A. Berlind and D. H. Weinberg, ApJ, **575**, 587 (2002), astro-ph/0109001.

[56] M. R. Blanton, D. W. Hogg, N. A. Bahcall, J. Brinkmann, M. Britton, A. J. Connolly, I. Csabai, M. Fukugita, J. Loveday, A. Meiksin, and et al., ApJ, **592**, 819 (2003), astro-ph/0210215.

[57] N. Padmanabhan, D. J. Schlegel, D. P. Finkbeiner, J. C. Barentine, M. R. Blanton, H. J. Brewington, J. E. Gunn, M. Harvanek, D. W. Hogg, Ž. Ivezić, and et al., ApJ, **674**, 1217 (2008), astro-ph/0703454.

[58] M. Tegmark, M. R. Blanton, M. A. Strauss, F. Hoyle, D. Schlegel, R. Scoccimarro, M. S. Vogeley, D. H. Weinberg, I. Zehavi, A. Berlind, and et al., ApJ, **606**, 702 (2004), astro-ph/0310725.

[59] F. James, *Statistical Methods in Experimental Physics: 2nd Edition, by Frederick James. ISBN-10 981-256-795-X; ISBN-13 981-270-527-9. Published by World Scientific Publishing Co., Pte. Ltd., Singapore, 2006.* (World Scientific Publishing Co, 2006).

[60] E. Calabrese, R. A. Hlozek, N. Battaglia, E. S. Battistelli, J. R. Bond, J. Chluba, D. Crichton, S. Das, M. J. Devlin, J. Dunkley, and et al., Physical Review D., **87**, 103012 (2013), arXiv:1302.1841 [astro-ph.CO].

[61] A. D. Montero-Dorta and F. Prada, MNRAS, **399**, 1106 (2009), arXiv:0806.4930.

[62] A. Kashlinsky, F. Atrio-Barandela, D. Kocevski, and H. Ebeling, ApJL, **686**, L49 (2008), arXiv:0809.3734.

[63] R. Keisler, ApJL, **707**, L42 (2009), arXiv:0910.4233 [astro-ph.CO].

[64] A. Kashlinsky, F. Atrio-Barandela, H. Ebeling, A. Edge, and D. Kocevski, ApJL, **712**, L81 (2010), arXiv:0910.4958 [astro-ph.CO].

[65] D. J. Eisenstein and W. Hu, ApJ, **496**, 605 (1998), astro-ph/9709112.

[66] N. Kaiser, H. Aussel, B. E. Burke, H. Boesgaard, K. Chambers, M. R. Chun, J. N. Heasley, K.-W. Hodapp, B. Hunt, R. Jedicke, and et al., in *Survey and Other Telescope Technologies and Discoveries*, Society of Photo-Optical Instrumentation Engineers (SPIE) Conference Series, Vol. 4836, edited by J. A. Tyson and S. Wolff (2002) pp. 154–164.

[67] N. Kaiser, W. Burgett, K. Chambers, L. Denneau, J. Heasley, R. Jedicke, E. Magnier, J. Morgan, P. Onaka, and J. Tonry, in *Ground-based and Airborne Telescopes III*, Society of Photo-Optical Instrumentation Engineers (SPIE) Conference Series, Vol. 7733 (2010).

[68] R. Laureijs, J. Amiaux, S. Arduini, J. . Augueres, J. Brinchmann, R. Cole, M. Cropper, C. Dabin, L. Duvet, A. Ealet, and et al., ArXiv e-prints (2011), arXiv:1110.3193 [astro-ph.CO].

[69] E. F. Schlafly, G. Green, D. P. Finkbeiner, M. Juric, H.-W. Rix, N. F. Martin, W. S. Burgett, K. C. Chambers, P. W. Draper, K. W. Hodapp, and et al., ArXiv e-prints (2014), arXiv:1405.2922.

[70] M. L. Balogh, D. Christlein, A. I. Zabludoff, and D. Zaritsky, ApJ, **557**, 117 (2001), astro-ph/0104042.

[71] H. J. Mo, X. Yang, F. C. van den Bosch, and Y. P. Jing, MNRAS, **349**, 205 (2004), astro-ph/0310147.

[72] D. J. Croton, G. R. Farrar, P. Norberg, M. Colless, J. A. Peacock, I. K. Baldry, C. M. Baugh, J. Bland-Hawthorn, T. Bridges, R. Cannon, and et al., MNRAS, **356**, 1155 (2005), astro-ph/0407537.

[73] C. Park, Y.-Y. Choi, M. S. Vogeley, J. R. Gott, III, M. R. Blanton, and SDSS Collaboration, ApJ, **658**, 898 (2007), astro-ph/0611610.

[74] P. Merluzzi, A. Mercurio, C. P. Haines, R. J. Smith, G. Busarello, and J. R. Lucey, MNRAS, **402**, 753 (2010), arXiv:0910.3877 [astro-ph.CO].

[75] A. Faltenbacher, A. Finoguenov, and N. Drory, ApJ, **712**, 484 (2010), arXiv:1002.0844 [astro-ph.CO].

[76] A. Nusser, E. Branchini, and M. Feix, JCAP, **1**, 018 (2013), arXiv:1207.5800 [astro-ph.CO].

[77] I. V. Chilingarian, A.-L. Melchior, and I. Y. Zolotukhin, MNRAS, **405**, 1409 (2010),

arXiv:1002.2360 [astro-ph.IM].
[78] D. Schlegel, F. Abdalla, T. Abraham, C. Ahn, C. Allende Prieto, J. Annis, E. Aubourg, M. Azzaro, S. B. C. Baltay, C. Baugh, and et al., ArXiv e-prints (2011), arXiv:1106.1706 [astro-ph.IM].
[79] M. Levi, C. Bebek, T. Beers, R. Blum, R. Cahn, D. Eisenstein, B. Flaugher, K. Honscheid, R. Kron, O. Lahav, and representing the DESI collaboration, ArXiv e-prints (2013), arXiv:1308.0847 [astro-ph.CO].
[80] M. Bilicki, T. H. Jarrett, J. A. Peacock, M. E. Cluver, and L. Steward, ApJ. S, **210**, 9 (2014), arXiv:1311.5246 [astro-ph.CO].